Desalination and Water Treatment
www.deswater.com

doi: 10.5004/dwt.2022.29118

280 (2022) 312–329
December

$CoFe_2O_4$@MC/AC as an efficient and recyclable magnetic nanohybrid adsorbent for the metronidazole removal from simulated wastewater: bioassays and whole effluent toxicity

Najmeh Golestani[a,b], Alireza Nasiri[a], Majid Hashemi[a,b,*]

[a]*Environmental Health Engineering Research Center, Kerman University of Medical Sciences, Kerman, Iran, Tel.: +98 3431325075; Fax: +98 3431325105; emails: mhashemi120@gmail.com/ma.hashemi@kmu.ac.ir (M. Hashemi), nasiri_a62@yahoo.com/ ARNasiri@Kmu.ac.ir (A. Nasiri)*
[b]*Department of Environmental Health Engineering, Faculty of Public Health, Kerman University of Medical Sciences, Kerman, Iran; email: n.golestani75@gmail.com (N. Golestani)*

Received 21 July 2022; Accepted 2 November 2022

ABSTRACT

$CoFe_2O_4$@methylcellulose (MC)/activated carbon (AC) as a novel magnetic nanohybrid adsorbent was synthesized and characterized with field-emission scanning electron microscope, energy-dispersive X-ray-mapping and linescan, X-ray diffraction, Fourier-transform infrared spectrometer, vibrating sample magnetometer, and Brunauer–Emmett–Teller techniques. Then, on synthetic and real samples, the adsorption process of metronidazole was investigated, and the parameters affecting the adsorption process were optimized. Finally, the toxicity of the effluent from the process was investigated. The maximum removal efficiency of metronidazole for synthetic and real wastewater samples was 93% and 85%, respectively, under optimal conditions of pH 3, adsorbent dose of 2.5 g/L, 10 mg/L initial concentration of metronidazole, temperature 25°C, and contact time of 20 min. The adsorption of metronidazole by $CoFe_2O_4$@MC/AC followed pseudo-second-order kinetic (R^2 = 0.999) and Freundlich isotherms (R^2 = 0.972). Furthermore, the thermodynamic findings of the process revealed ΔH = –19.82 (kJ/mol) and ΔS = –53.57 (J/mol·K), as well as negative Gibbs free energy values, indicating that the process was spontaneous and exothermic. After four regeneration cycles, the $CoFe_2O_4$@MC/AC was able to remove 66% of metronidazole while maintaining high chemical stability. The effects of effluent toxicity on *Daphnia* and *Artemia* were enhanced by increasing effluent concentration and exposure duration, according to the LC_{50} values. However, the mortality rate for *Daphnia* and *Artemia* after 72 h at the maximum effluent concentration (100% by volume) was 33.3% for *Daphnia* and 26.6% for *Artemia*, according to the results. According to the findings, $CoFe_2O_4$@MC/AC can be employed as a novel magnetic nanoadsorbent with a high adsorption ability to eliminate pharmaceutical pollutants from aqueous solutions.

Keywords: Magnetic nano-biosorbent; Metronidazole; Toxicity; *Daphnia*; *Artemia*

1. Introduction

Water supplies are in great jeopardy today as a result of population increase, pollution, and climate change. The release of industrial effluents including organic and inorganic chemicals into natural ecosystems is one of the most significant sources of pollution. Drugs are one of the most persistent pollutants in wastewater, which has prompted a greater focus on the presence of various drug groups in aquatic ecosystems. Agricultural runoff, direct

* Corresponding author.

disposal from municipal and hospital wastewater treatment facilities, direct disposal of medical, veterinary, and industrial waste, and disposal of expired pharmaceuticals are all ways that drugs are imposed on the ecosystem [1,2]. Drugs that are discharged into the environment can go up the food chain, with varying degrees of toxicity depending on the compound. However, while the quantity of these chemicals in water is relatively low (around nanograms or micrograms per liter), their build-up in poultry, animals, and plants can eventually cause diseases in living organisms [3].

Antibiotics, which are commonly used to treat diseases caused by parasites and anaerobic bacteria such as *Giardia lamblia*, *Helicobacter pylori*, and *Trichomonas vaginalis*, are among the pharmaceutical compounds [2,3]. Some of these compounds' metabolites are excreted from the body and discharged into the environment because they are not fully digested in the human body. This raises major concerns about the safety of drinking water, highlighting the need of identifying and removing harmful chemicals from aquatic habitats. Antibiotics in the raw wastewater treatment plant units, on the other hand, might generate undesirable by-products during the chlorination and ozonation stages of water. These compounds are classified as probable human carcinogen and mutant due to lymphocyte damage, and they must be removed from the effluent before it is discharged into the environment [3].

Metronidazole is a 5-nitroimidazole derivative from the first generation having strong antibacterial properties against trichomonas, anaerobic bacteria, giardiasis, and amoebiasis. Metronidazole can found in hospital wastewater in concentrations ranging from 1.8 to 9.4 μg/L. Although the amount of metronidazole in the aquatic environment is low, it is considered an emerging environmental pollutant since its continued introduction might provide a long-term threat to living species [4,5].

Antibiotics can be eliminated using a variety of physical, chemical, and biological techniques, depending on the chemical and physical features of the pollutants [3,5,6]. UV photolysis [7], surface adsorption [8–10], biodegradation [11], photocatalytic degradation [12,13], chemical oxidation [14–17] during Fenton processes [18], photo Fenton [19,20], electro-Fenton [15], photo-electro-Fenton [21], ozonation [22], and catalytic ozonation [23] are some examples of these techniques. Despite their benefits, each of these techniques has disadvantages that make their usage challenging in most circumstances. Compounds are utilized as oxidants in chemical processes, particularly advanced oxidation [24–29], which are generally expensive, damaging to equipment, poisonous, and produce compounds and by-products with higher toxicity [30]. The removal effectiveness of physical techniques such as microfiltration [31], ultrafiltration [32], nanofiltration [31], and reverse osmosis is high, but the maintenance of these systems is expensive, and the membranes become clogged and damaged throughout the process [33]. High doses of antibiotics induce toxicity to the microorganisms utilized in the treatment and biomass formation throughout the treatment process in biological approaches such as activated sludge [34].

The adsorption process is a promising process to reduce pollutants such as medicinal, heavy metals, and dye compounds due to low operating costs, high flexibility, insensitivity of the process to toxic compounds and pollutants, no secondary pollution in the system, the possibility of adsorbent separation, efficiency, and high specific level for removal [35–37]. Solid porous adsorbents perform the majority of adsorption processes, and many adsorbents are produced with pores in the nanoscale range [38,39]. Because of their large surface area and active sites, nanomaterials have a high adsorption capability [40–43]. Magnetic nanoadsorbents can also be separated and reused in the past [44–46]. The adsorption process is greatly aided by selecting the appropriate adsorbent [36,47–51]. Activated carbon [52–58], graphene oxide [59], clay minerals [60], organic metal frames [59], and biochar have all been utilized as adsorbents to remove different antibiotics and pollutants [61]. They can eliminate various chemical pollutants because of their low toxicity, availability, ease of access, and cost-effectiveness.

In the production and synthesis of magnetic compounds, iron oxides and other ferrite compounds have gotten a lot of interest [62]. Magnetic adsorbents are materials that have found a suitable role in water treatment because of their high adsorption effectiveness, inexpensive production costs, fast separation, minimal pollutant generation, and ability to treat a large volume of water in a short period [63,64]. Among the magnetic nanoadsorbents utilized thus far are (MOF@GO) [65], (SF-Fe_3O_4-EDTA) [66], ($CoFe_2O_4$@γ-Fe_2O_3) [67], Zn–Fe (thioglycolic-modified Zn–Fe layer double hydroxide) [68], ($CoFe_2O_4$@SiO_2-C_8) [69], (GO/g-C_3N_4-Fe_3O_4) [70], Fe_3O_4@SiO_2@CS/GO [71], Ni/HAP/$CoFe_2O_4$ [72], AC-Fe_3O_4 [73].

It is critical to incorporate biological components in the synthesis of these magnetic nanoadsorbents to optimize their performance and structure. Cellulose is a polysaccharide made up of a linear carbohydrate chain formed of hundreds to thousands of glucose units. Cellulose is the most prevalent and accessible natural biopolymer, and it is one of the most essential structural components of the main cell wall of green plants and a variety of algae. Methylcellulose is one of the cellulose ether derivatives, which is mainly composed of glucose units bonded together by alpha-beta-glycosidic bonds [74]. Cellulose-derived carbohydrate biopolymers such as methylcellulose, carboxymethylcellulose, and chitosan are biodegradable, low-cost, readily accessible, renewable, stable, non-toxic, high-permeability compounds with numerous uses in water and wastewater treatment processes. Despite all of the benefits, separating these biopolymers from the purification process necessitate time-consuming centrifugation and filtration techniques [75,76]. By magnetizing these polymeric carbohydrates and synthesizing ferrite nano-biocomposites, this problem can be overcome. Other ferrite nano-biocomposites derivatives, such as $CoFe_2O_4$@MC, $CuFe_2O_4$@MC, $ZnFe_2O_4$@MC, and $ZnFe_2O_4$@CMC, have been synthesized recently, and their physical and chemical characteristics have been investigated and confirmed, and also these ferrite nanocomposites have been employed in the treatment of water and wastewater [25,26,77–84].

Despite the high effectiveness of magnetic nanoadsorbents, attention should be paid to the environmental issue of effluent entrance into the environment as well as the toxicity of these compounds. When this effluent comes into interaction with biological ecosystems, it may exhibit a variety of behaviors, indicating the necessity to investigate the

effluent's toxicity from several perspectives. If this effluent is not assessed for toxicity before entering the food chain, it might produce acute, chronic, or long-term negative effects. They also get into cells and internal components like mitochondria and nuclei, causing oxidative damage to the cell surface and genetic damage through direct and indirect methods [85]. As a result, the risk of these compounds contaminating humans has grown, and their potential toxicity should be considered and investigated [86].

Experiments that employ living organisms as biomarkers for measuring the toxicity of chemicals are known as biometrics or bioassays [87]. The bioassay of many organisms such as fish, algae, bacteria, and freshwater and marine organisms such as *Artemia* [88] and *Daphnia* [89], are widely used to identify the toxicity of chemicals and evaluate the toxicity of leachate, municipal and industrial wastewater, and the quality of water resources [90]. In addition to cheap cost, short test time, simplicity, and low-test cost, the use of these two aquatic organisms in bioassays is also very sensitive [88]. *Artemia* belongs to the arthropod branch, crustacean, end gill subspecies, uncovered order, *Branchiothidae* family, and genus *Artemia*, and is a biomarker of high salinity waters. This crustacean's larval stages are extremely sensitive to pollutants and chemicals in the environment [88]. *Daphnia* is another well-known and commonly utilized organism in bioassay. *Daphnia* babies range in size from 0.8 to 1 mm in length and are visible to the naked eye. At this stage of the life cycle, *Daphnia* is highly essential in bioassay investigations [91]. *Artemia* grows in brackish and brackish water, whereas *Daphnia* lives in freshwater. As a result, they exhibit varying levels of resistance and susceptibility to environmental stimuli. As a result, these two types of water were examined in the current study's bioassay test of the effluent produced by this process.

According to previous studies, $CoFe_2O_4$@MC/AC magnetic nano-biocomposite has not been synthesized in a green and ecologically friendly manner, and it has not been evaluated for the removal of metronidazole antibiotic. The purpose of this study was to synthesize $CoFe_2O_4$@MC/AC magnetic nano-biocomposite by co-precipitation technique assisted with microwaves as a magnetic nanoadsorbent, to characterize the structure of this nanoadsorbent, and to evaluate its effectiveness in adsorbing the antibiotic metronidazole from aqueous environments through the adsorption process. Subsequently, using a bioassay approach on two aquatic organisms including *Daphnia* living in fresh water and *Artemia* living in salt and brackish water, the toxicity level of magnetic nanoadsorbent and the effluent from the process was also assessed.

2. Materials and methods

2.1. Chemicals and instruments

All chemicals and reagents including iron(III) chloride hexahydrate ($FeCl_3{\cdot}H_2O$), cobalt(II) chloride hexahydrate ($CoCl_2{\cdot}6H_2O$), methylcellulose (MC), sodium hydroxide (NaOH), and activated carbon (AC) were purchased from Sigma-Aldrich Co. Deionized water was used during the experiments. HCl and NaOH were used for adjusting the solution pH. In this study, devices such as a spectrophotometer (SHIMADZU, UV-1800), microwave (SAMSUNG, 2450MHz, 800W), and pH meters (HANNA instruments, pH 212) were used.

2.2. Preparation of $CoFe_2O_4$@MC/AC

Stoichiometric amounts of metals chloride and MC were separately dissolved in 100 mL of deionized water. Then 6 g of NaOH was added for 1 hr. to alkalize the pH of the solution. In the final stages of the synthesis, 1 g of activated carbon was added to the reaction container and stirred. After adding activated carbon to the solution, the mixture was placed in the microwave oven at 450 W 3 times for 5 min to obtain a black precipitate. The obtained precipitate was separated using a magnet and washed several times with deionized water to neutralize the final pH. Finally, the black precipitate was dried for 24 h at 70°C temperature in the furnace (Fig. 1).

2.3. Batch adsorption experiments

At first, MNZ stock solution was made with a concentration of 100 mg/L and then concentrations of 10, 15, 20, 30,

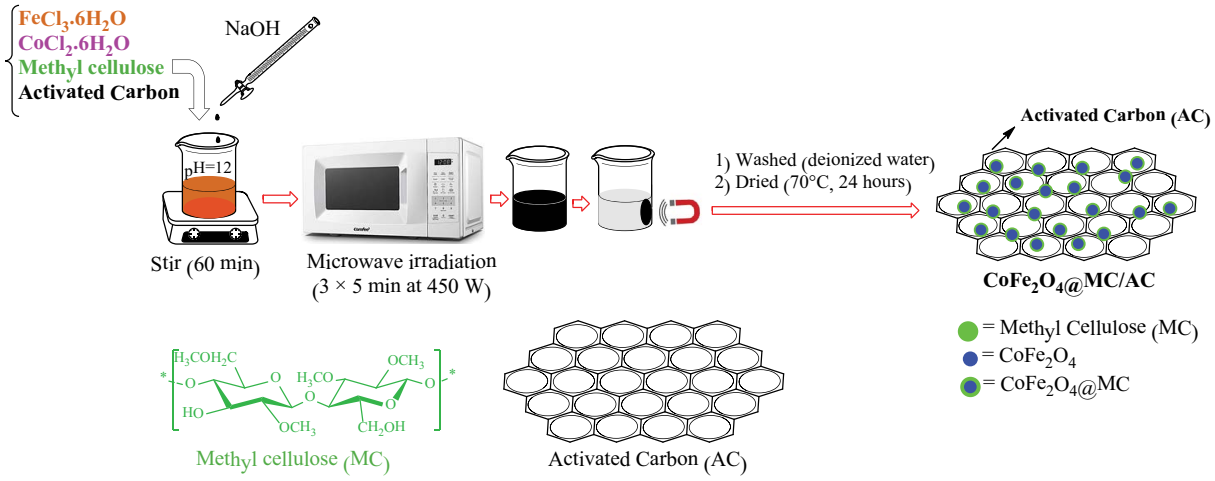

Fig. 1. Schematic of $CoFe_2O_4$@MC/AC preparation.

and 40 mg/L were prepared from it. To optimize the adsorbent dose, amounts of 1–3 g/L were investigated. Solutions of 1 N NaOH and HCl were used to adjust the pH and pHs of 3, 5, 7, 9, and 11 were surveyed. Contact times of 20 min and temperatures of 25°C, 30°C, 35°C, 40°C, and 60°C were investigated and optimized. Finally, the adsorption efficiency [Eq. (1)], and adsorption capacity [Eq. (2)], were calculated by the following formulas:

$$R_e(\%) = \frac{C_0 - C_t}{C_0} \times 100 \tag{1}$$

where R_e: adsorption efficiency (%); C_0 and C_t: initial and final concentrations (mg/L), respectively.

$$Q_e = \frac{(C_0 - C_t)V}{m} \tag{2}$$

where Q_e: adsorption capacity; C_0 and C_t: initial and final concentrations (mg/L), respectively; V: volume of solution (L); m: adsorbent mass (g).

2.4. Regeneration experiments (reusability and chemical stability)

The adsorbent was gathered by a magnet from the process medium and placed in a furnace at 200°C for 1 h to assess the regenerability of the nanoadsorbent utilized. Then the efficacy of the adsorbent under optimal conditions for metronidazole removal was investigated for four cycles.

2.5. Adsorption isotherm models

The Langmuir and Freundlich isotherms were used to assess the equilibrium state throughout this procedure. Adsorption occurs in a single layer in the Langmuir model [Eq. (3)], with the adsorbed molecule on the adsorbent surface with constant adsorption energy, and adsorption of one molecule in an adsorption site does not affect the adsorption of additional molecules.

$$\frac{C_e}{Q_e} = \frac{1}{Q_{\max} K_L} + \frac{C_e}{Q_{\max}} \tag{3}$$

where $q_{\max}$ (mg/g) represents the maximum adsorption capacity, C_e (mg/L) represents the metronidazole equilibrium concentration, Q_e (mg/g) represents the amount adsorbed at equilibrium, and K_L represents the Langmuir coefficient.

R_L [Eq. (4)] is another metric that investigates the adsorption process. As a result, the adsorption process is irreversible if $R_L = 0$, the ideal adsorption process if $0 < R_L < 1$, the adsorption process is linear if $R_L = 1$, and the adsorption process is undesirable if $R_L > 1$.

$$R_L = \frac{1}{1 + K_L C_0} \tag{4}$$

where K_L is the Langmuir constant, and C_0 is the initial metronidazole concentration in mg/L [92].

For multilayer adsorption with heterogeneous heat distribution and adsorption on heterogeneous surfaces, the Freundlich model [Eq. (5)] can be utilized.

$$\log q_e = \log k_f + \frac{1}{n} \log C_e \tag{5}$$

The adsorption capacity is represented by k_f (mg/g) (1/mg) in this equation. $1/n$ is a heterogeneity factor or surface adsorption intensity that specifies the kind of isotherm, with $1/n = 0$ indicating reversible adsorption, $1 < 1/n < 0$ indicating favorable adsorption, and $1/n > 1$ indicating undesirable adsorption [93].

2.6. Kinetic study

To better understand the dynamics and effects of variables impacting the rate of metronidazole adsorption on the adsorbent, the adsorption kinetics of metronidazole were studied using pseudo-first-order [Eq. (6)] and pseudo-second-order [Eq. (7)] kinetic models.

$$\ln(q_e - q_t) = \ln q_e - K_1 t \tag{6}$$

The rate constant of the pseudo-first-order model is K_1 in this equation. The amounts of metronidazole adsorbed at equilibrium and at particular times (min) are shown in q_e and q_t, respectively.

$$\frac{t}{q_t} = \frac{1}{K_2 q_e^2} + \frac{1}{q_e} \times t \tag{7}$$

where K_2 is a kinetic constant of pseudo-second-order. The amounts of metronidazole adsorbed at equilibrium and at particular times (min) are represented by q_e and q_t (mg/g). The slope of the line graph of Eq. (7) can be used to calculate the rate constant K_2 [94].

2.7. Thermodynamic study

Thermodynamic factors such as Gibbs free energy (ΔG), enthalpy (ΔH), and entropy (ΔS) changes can be studied using constant equilibrium changes with equilibrium temperature. Eq. (8) calculates the Gibbs free energy changes in the adsorption process.

$$\Delta G = -RT \ln k_d \tag{8}$$

where ΔG (kJ/mol) is the Gibbs free energy change, R is the general constant of gases with the value 8.314 (J/mol·K), and temperature in Kelvin. Eq. (9) is also used to compute the equilibrium constant.

$$K_d = \frac{V}{W} \times \frac{(C_0 - C_e)}{C_e} \tag{9}$$

where C_e (mg/L) and C_0 (mg/L) are the initial and equilibrium concentrations, respectively, with V (mL) representing the

volume of the solution and W (g) representing the mass of the adsorbent [95,96].

2.8. pH_{zpc} determination

50 mL of KCl 0.1 M solutions at six different pH (2, 4, 6, 8, 10, and 12) and 0.01 g of magnetic nanoparticles were applied to the determination of pH_{zpc}. Then the prepared solutions place on the shaker and measured the final pH after 24 h. $\Delta pH = pH_{final} - pH_{initial}$ was calculated and its curve was plotted as the $X = pH_{initial}$ and $Y = \Delta pH$. The intersection of the curve with the X-axis is equal to pH_{zpc} [78].

2.9. Toxicity evaluation

The toxicity of the process effluent was assessed using *Daphnia* and *Artemia*. *Daphnia* and *Artemia* were first propagated in growth-friendly conditions. *Daphnia* culture medium was made by combining 5 g of dry sheep manure, 25 g of garden soil, and 1 L of spring water according to the conventional procedure to produce *Daphnia* babies. Several mature *Daphnia* were propagated by transferring them to the culture medium. After then, the babies were born, cared for, and fed. Dry yeast was utilized to feed *Daphnia* regularly, and the aquarium was slowly aerated with an aquarium air pump [97].

To assess *Artemia* toxicity, *Artemia* eggs were hatched at pH 7.8, 27°C, and 2,000 lux light. Because *Artemia* is a saline aquifer, the utilized water was synthetic saline water (1 L piped water with 30 g of sea salt), which was vigorously aerated for a week to dechlorinate. The *Artemia nauplii* hatched 24 h after the addition of *Artemia* eggs, and due to light exposure, the *Artemia nauplii* were placed in a container in a dark spot so that healthy and mobile babies may congregate on the container's surface and be collected using a Pasteur pipette [88].

Finally, samples with various dilutions of 0, 10, 25, 50, 75, and 100 mg/L were prepared from the process effluent and a certain number of *Daphnia* (30) and *Artemia* (30) were added to these samples to determine the toxicity of the effluent from the process following the Organization for Economic Cooperation and Development's (OECD) standard guideline No. 202 [98]. The mortality rate of these two aquatic species was next investigated at 12, 24, 36, and 48 h. Immobile aquatic species were enumerated and recorded as dead after contact with certain concentrations of effluent from the process, and the LC_{50} quantity of effluent was computed using a probit test in SPSS software [99].

3. Results and discussion

3.1. Characterization of the synthesized magnetic nanoadsorbent

Initially, the novel magnetic nanoadsorbent $CoFe_2O_4$@MC/AC was prepared from Co^{2+} and Fe^{3+} with the existence of MC and AC by using a new microwave-assisted technique based on the experimental procedure. To characterize this magnetic nanoadsorbent, several techniques were applied. This black precipitate, which acts as a magnetic nanoadsorbent, was structurally characterized by X-ray diffraction (XRD; PHILIPS PW1730), Fourier-transform infrared spectroscopy (FTIR; AVATAR, Thermo), field-emission scanning electron microscope (FESEM; TESCAN MIRA III), energy-dispersive X-ray (EDS)-mapping and Linescan (TESCAN MIRA II, SAMX Detector), Brunauer–Emmett–Teller (BET; BELSORP MINI II) and vibrating sample magnetometer (VSM; LBKFB, BEAMGOSTAR TABAN Company) devices. After confirming the physical and chemical structure of the magnetic nanoadsorbent, this compound was used as an adsorbent in the MNZ removal process.

To determine the morphology and size, the FESEM images of the produced $CoFe_2O_4$@MC/AC were illustrated. Fig. 2a depicts the FESEM images of $CoFe_2O_4$@MC/AC synthesized in the presence of methylcellulose as a biopolymer. The impact of methylcellulose on the morphology of $CoFe_2O_4$@MC/AC formed smoothly, uniformly, and loosely aggregated pseudo spherical shape magnetic nanoadsorbent (~11 nm), even in the composite structure.

Mapping and line scanning were used to investigate the $CoFe_2O_4$@MC/AC magnetic nanoadsorbent element distribution (Fig. 2b and c). Based on the obtained results shown in Fig. 4a (mapping), Co, Fe, O, and C had a homogeneous distribution that indicates high uniformity of the synthesized $CoFe_2O_4$@MC/AC. Also, line scanning which showed in Fig. 4b has confirmed these results.

The synthesized $CoFe_2O_4$@MC/AC purity and chemical structure were evaluated by EDS analysis (Fig. 2d) The EDS results demonstrate 34.71% Fe, 32.21% O, 19.18% Co, and 13.89% C in the chemical structure of $CoFe_2O_4$@MC/AC magnetic nanoadsorbent which were following the expected values.

Fourier-transform infrared spectroscopy (FTIR) has been used to obtain the functional group of synthesized nanoparticles. By using a KBr disc, the powdered $CoFe_2O_4$@MC/AC was investigated (Fig. 3).

Fig. 3 presents a comparison of the KBr pellet for the FTIR spectra of MC and $CoFe_2O_4$@MC/AC to obtain the functional group of synthesized nanoparticles. Based on FTIR spectra, the MC vibrational absorption bands were as follows: C–H stretching at >3,000 cm^{-1}, O–H stretching at 3,461 cm^{-1}, adsorbed water stretching at 1,644 cm^{-1}, C–O stretching at 1,100–1,150 cm^{-1}, C–H bending of methyl and methylene groups at 1,377 and 1,457 cm^{-1}, and C–O–C stretching vibration of the methylcellulose glycosidic bond at 1,066 cm^{-1} respectively [100–104]. As well, two confirming absorption peaks of the metal spinel ferrite structure were seen at 434 and 601 cm^{-1} which demonstrated the metal cation at the octahedral site M_{octa}-O and the intrinsic stretching vibrations of the metal cation at the tetrahedral site M_{tetra}-O, respectively.

XRD analysis was used to characterize structures, phases, and crystalline composition of $CoFe_2O_4$@MC/AC. The achieved results are shown in Fig. 4.

The XRD pattern of AC and MC presented a prominent peak centered at 11.00° and 18.23°, respectively. Based on the JCPDS 96-591-0064, the $CoFe_2O_4$@MC/AC crystal phase structure and XRD pattern with diffraction peaks at 2θ = 29.98°, 35.31°, 42.95°, 53.47°, 56.82°, 62.47°, and 74.15° are indexed to the $CoFe_2O_4$ cubic spinel phase [78]. According to the obtained results, the $CoFe_2O_4$ crystal structure was well protected in the MC and AC composition. It was so interesting that the XRD spectrum of $CoFe_2O_4$@MC/AC indicated the characteristic peaks linked with both MC and

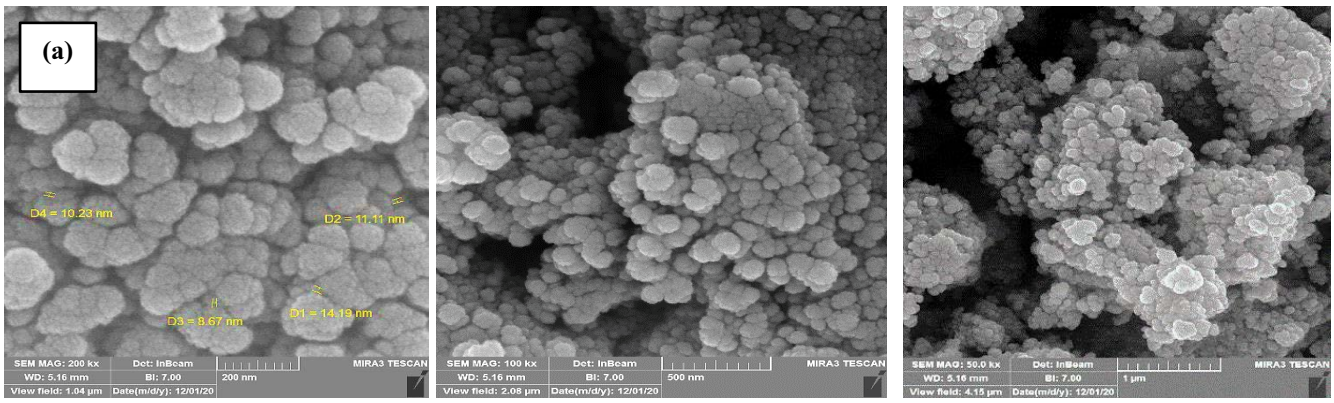
(a)
D4 = 10.23 nm
D2 = 11.11 nm
D3 = 8.67 nm
D1 = 14.19 nm
SEM MAG: 200 kx
Det: InBeam
WD: 5.16 mm
BI: 7.00
200 nm
MIRA3 TESCAN
View field: 1.04 µm
Date(m/d/y): 12/01/20
SEM MAG: 100 kx
Det: InBeam
WD: 5.16 mm
BI: 7.00
500 nm
MIRA3 TESCAN
View field: 2.08 µm
Date(m/d/y): 12/01/20
SEM MAG: 50.0 kx
Det: InBeam
WD: 5.16 mm
BI: 7.00
1 µm
MIRA3 TESCAN
View field: 4.15 µm
Date(m/d/y): 12/01/20

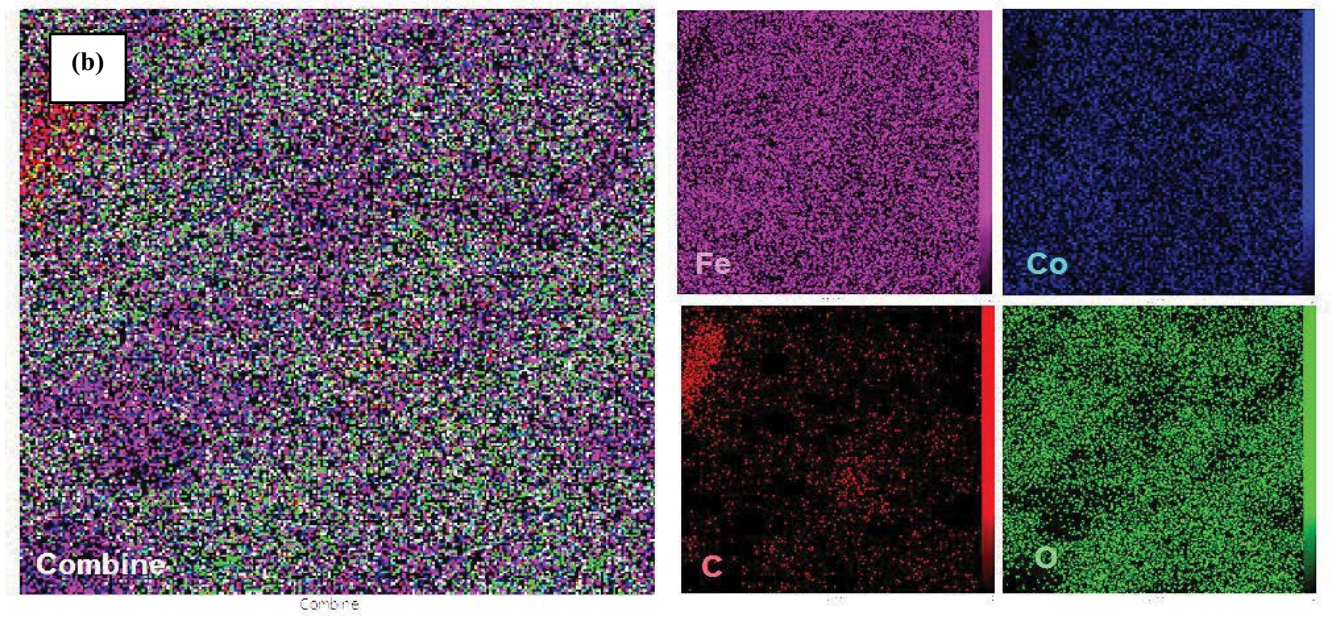
(b)
Combine
Fe
Co
C
O

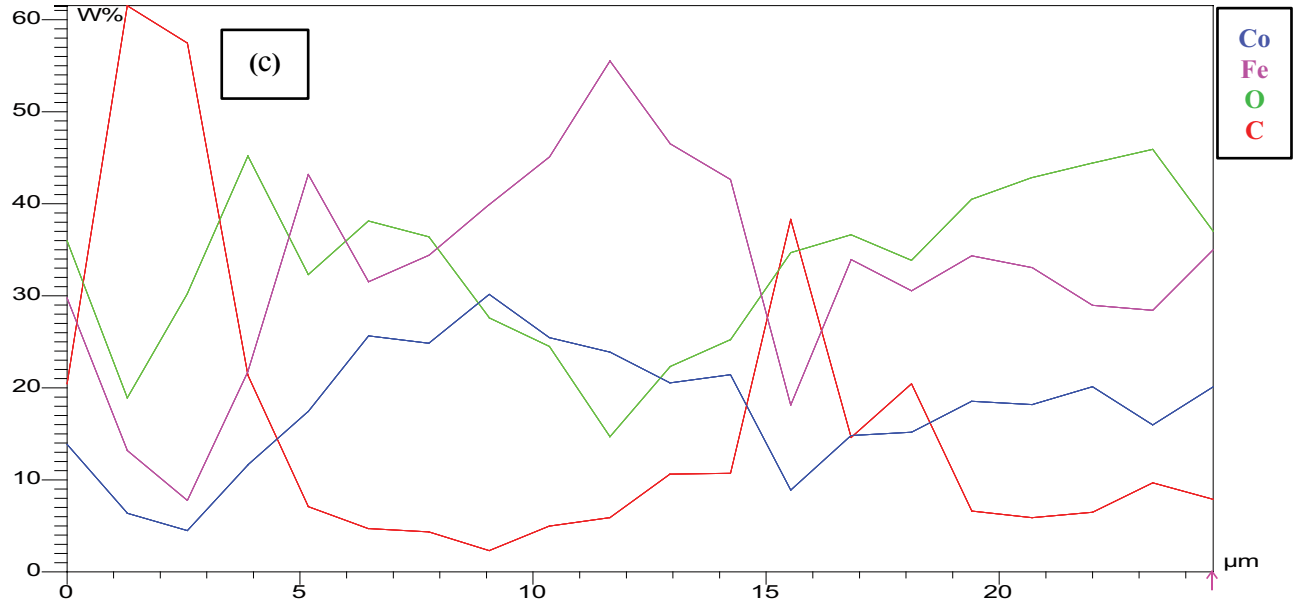
(c)
W%
60
50
40
30
20
10
0
0
5
10
15
20
µm
Co
Fe
O
C

(Continued)

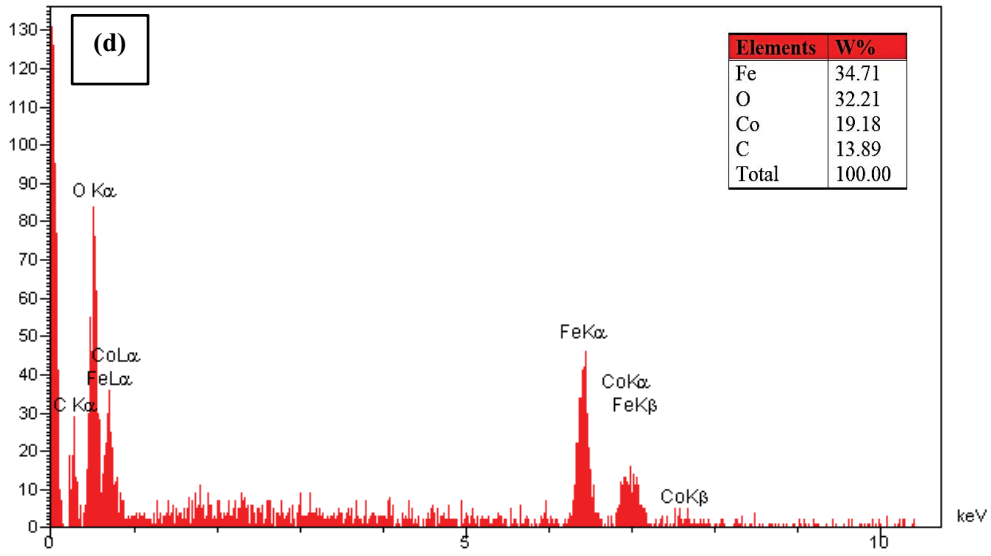

Fig. 2. FESEM (a), mapping (b), line scanning (c), and EDS (d) of $CoFe_2O_4$@MC/AC magnetic nanoadsorbent.

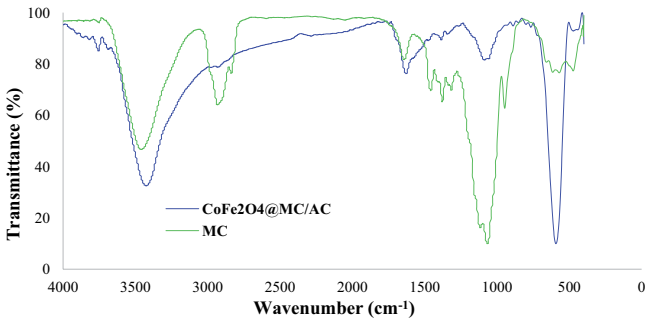

Fig. 3. FTIR of $CoFe_2O_4$@MC/AC magnetic nanoadsorbent and MC.

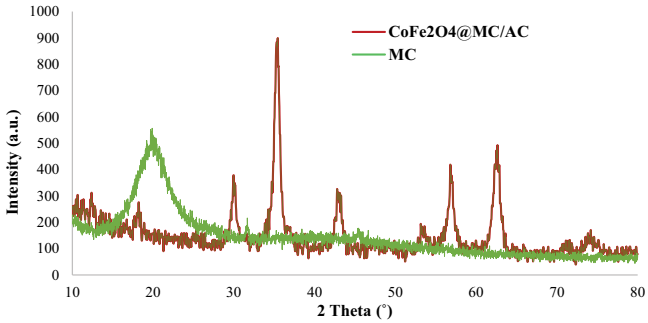

Fig. 4. XRD patterns of $CoFe_2O_4$@MC/AC magnetic nanoadsorbent and MC.

AC and $CoFe_2O_4$, which points to the successful synthesis of $CoFe_2O_4$@MC/AC magnetic nanoadsorbent.

Fig. 5 shows the adsorption/desorption isotherm and BET-plot specific surface area of the synthesized $CoFe_2O_4$@MC/AC (Fig. 5a and b).

According to the BET plot the specific surface area, mean pore diameter, and total pore volume (p/p_0 = 0.99) of synthesized magnetic nanoadsorbent were obtained 128.22 m^2/g, 7.1194 nm, and 0.2282 cm^3/g, respectively. According to the IUPAC, pores are arranged into three groups: microporous, mesoporous, and macroporous materials [105]. Based on the IUPAC definition, the mesoporous material is a material including pores with diameters between 2 and 50 nm. Also, the pores sizes of microporous and macroporous are smaller than 2 nm and larger than 50 nm, respectively [105]. $CoFe_2O_4$@MC/AC could be classified as a mesoporous material.

By using a vibrating sample magnetometer, The $CoFe_2O_4$@MC/AC magnetic nanoadsorbent property was investigated (Fig. 6)

The remnant magnetization (Mr), saturation magnetization (Ms), and coercive force (Hc) values were obtained as 15.46 emu/g, 57.91 emu/g, and 400 Oe, respectively (Fig. 8). These values were evidence for the $CoFe_2O_4$@MC/AC magnetic nanoadsorbent which has high magnetic strength. The results demonstrated that the $CoFe_2O_4$ magnetic property in the $CoFe_2O_4$@MC/AC structure is preserved.

3.2. Adsorption test optimization

3.2.1. Effect of adsorbent dose

Fig. 7a shows the influence of the nanoadsorbent dosage on metronidazole removal efficiency after 70 min. At initial concentrations of 10 mg/L metronidazole, pH 3, and 25°C, nanoadsorbent dosages of 1, 1.5, 2, 2.5, and 3 g/L were investigated. According to the findings, increasing the quantity of nanoadsorbent from 1 to 3 g/L improved the antibiotic removal efficiency from 35% to 69%. This might be caused to an increase in the amount of adsorbent contact and the number of adsorption sites available [106]. The removal efficiency of metronidazole rose from 65% to 69% after increasing the quantity of adsorbent from 2.5 to 3 g/L, indicating that 2.5 g/L was the optimum dosage of nanoadsorbent. Guo et al. [107] showed that increasing the

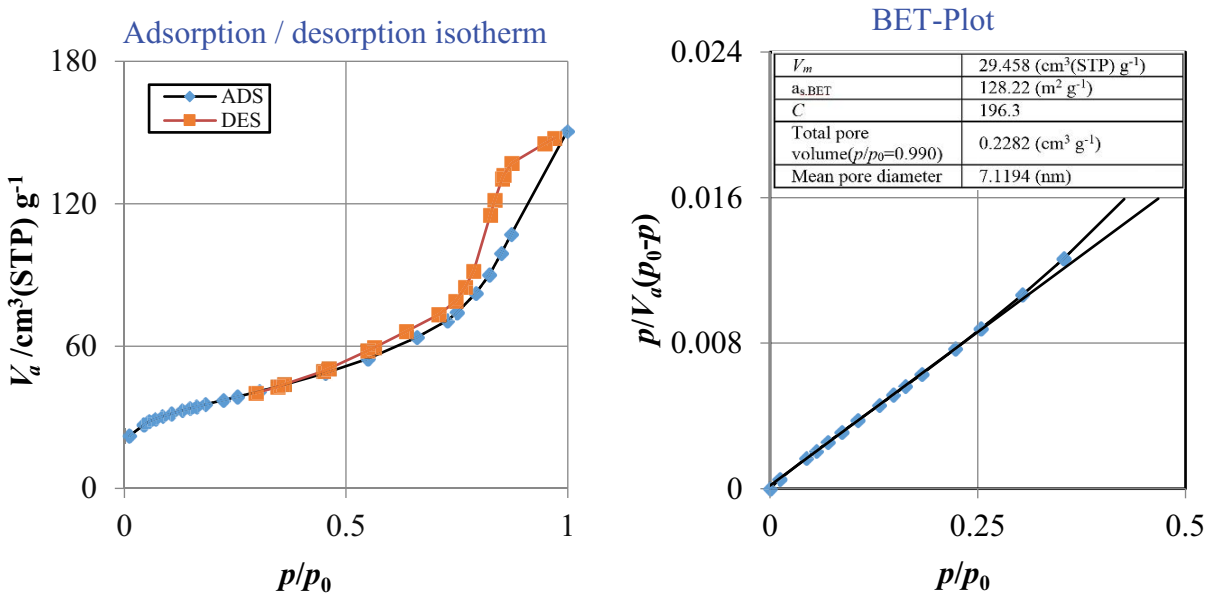

Fig. 5. Adsorption/desorption isotherm (a) and BET surface area (b) of $CoFe_2O_4$@MC/AC magnetic nanoadsorbent.

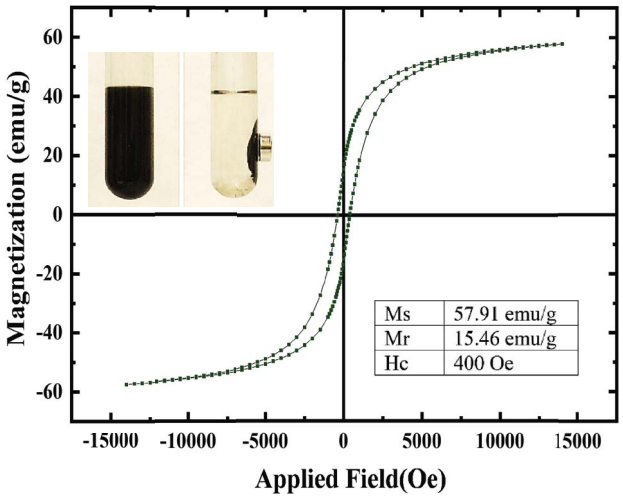

Fig. 6. VSM magnetization curve of $CoFe_2O_4$@MC/AC magnetic nanoadsorbent; the photo inset shows the solution after magnetic separation of the magnetic nanoadsorbent.

adsorbent dosage from 0.1 to 1 g/L increased the removal efficiency from 47% to 98%, which was consistent with the findings of this study.

3.2.2. Effect of the initial concentration

Concentrations of 10, 15, 20, 30, and 40 mg/L were evaluated to optimize the concentration of metronidazole in the adsorption process. The adsorption efficiency of metronidazole decreases from 93.5% to 77% when the initial concentration of the solution is increased from 10 to 40 mg/L, as illustrated in Fig. 7b. As a result, the optimum metronidazole concentration was 10 mg/L. The decrease in metronidazole removal efficiency with increasing its concentration is because as the initial concentration rises, the density of pollutant molecules in the environment rises, causing the active sites on the adsorbent surface to become occupied, so lowering metronidazole removal efficiency [108]. The adsorption of metronidazole from wastewater using a floating bed reactor by iron and coal was also reported by Malakootian et al. [5], who found that when the concentration of metronidazole increases, the removal efficiency declines, which was consistent with the findings of this work.

3.2.3. Effect of temperature

Another aspect that affects the adsorption process is the process temperature. Fig. 7c depicts the influence of temperature fluctuations on metronidazole adsorption efficiency. Temperatures ranging from 25°C to 60°C were investigated in this study. The findings of the investigation of the influence of process temperature on metronidazole removal efficiency indicated that at 25°C, metronidazole removal efficiency by nanoadsorbent is 93%, whereas as the temperature increased to 60°C, metronidazole removal efficiency declined to 87%. The adsorption process is exothermic, according to this conclusion. A similar result was observed in Sun et al. [109] study for metronidazole removal, which was compatible with the findings of this investigation.

3.2.4. Effect of pH

The impact of pH on the adsorption process is significant. The findings of the influence of pH on the removal efficiency of metronidazole by magnetic nanocomposite at an initial concentration of 10 mg/L, the nanoadsorbent dose of 2.5 g/L, as well as contact time of 70 min are presented in (Fig. 7d). According to the results, the highest removal efficiency of metronidazole was 80% at pH = 3. On the other hand, it was found that by increasing the pH from 3 to 9, the removal efficiency decreases to 62%, so pH = 3

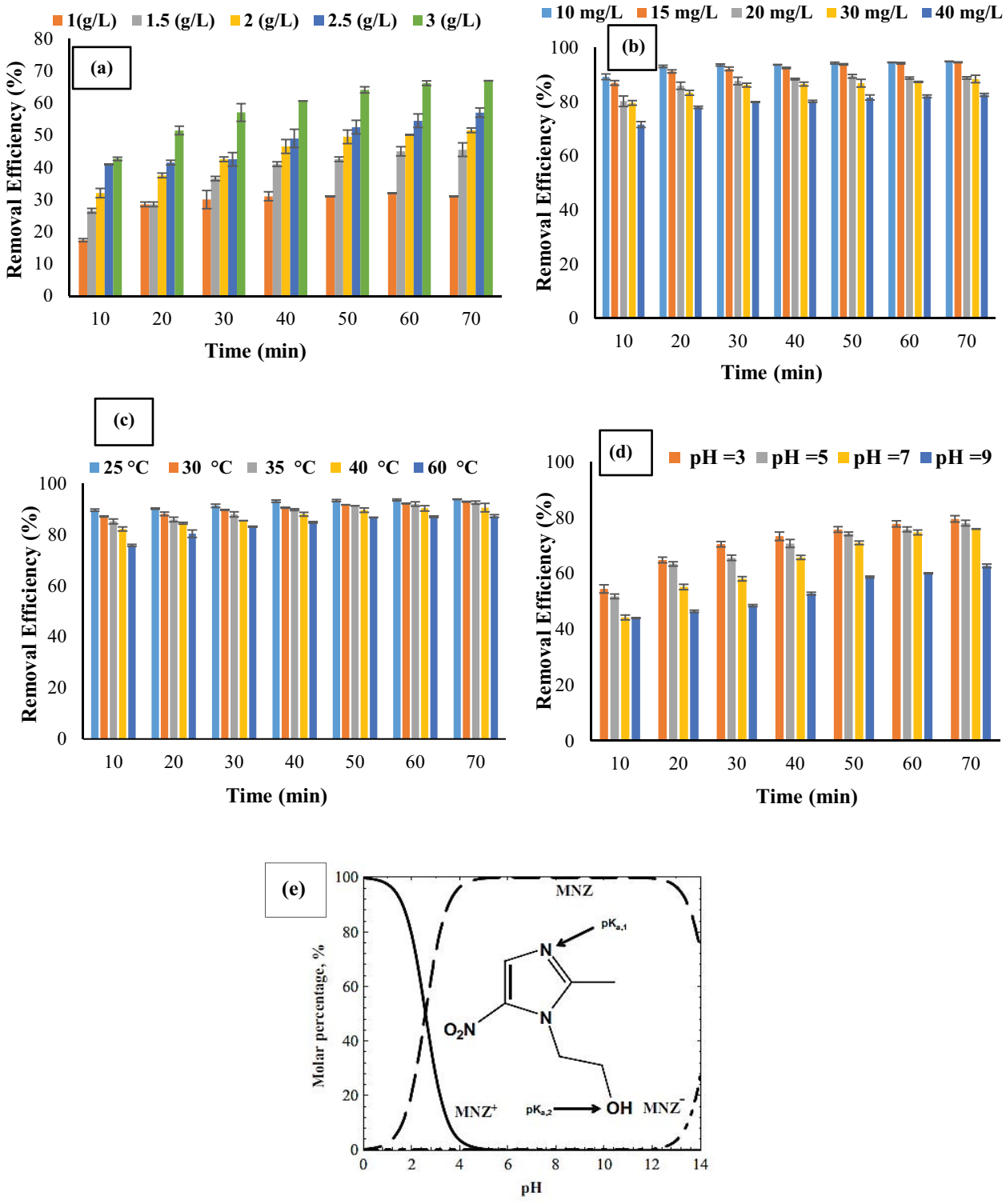

Fig. 7. Effect of nanoadsorbent amount (a), metronidazole concentration (b), temperature (c), pH (d) and pKa metronidazole (e) on metronidazole removal efficiency (temperature = 25°C, pH = 3, dosage nanoadsorbent = 2.5 g/L, concentration MNZ = 10 mg/L).

was considered the optimal pH. Using electrostatic and lyophobic forces, the adsorption behavior of metronidazole on the adsorbent surface was investigated. Metronidazole has two pKa, as shown in Fig. 7e. The five-ring nitrogen is represented by pKa_1 = 2.55, whereas the hydroxyl group is represented by pKa_2 = 14.44. In the pH range of 4 to 12, metronidazole becomes closer to the anionic form as the pH rises, but at pHs lower than 4, the cationic form

predominates. Given that the study's optimal pH was 3, metronidazole may be expected to be present in cationic form. The pH_{zpc} of $CoFe_2O_4$@MC/AC magnetic nanocomposite, on the other hand, was measured and found to be 6.5. According to pH_{zpc}, the adsorbent's surface charge is negative at pHs more than 6.5 and positive at pHs less than 6.5. Since the optimal pH of process 3 is already, the adsorbent's surface has a positive charge, causing electrostatic repulsion with the positive charge of metronidazole. Although metronidazole is an organic component in the aqueous medium, it tends to separate from the solution and reach the adsorbent surface under the influence of lyophobic forces under these circumstances, and this process is dominant [110]. Similar results were found in research on metronidazole adsorption done by Malakootian et al. [26]. They also discovered that metronidazole removal efficiency was greater at acidic pHs.

3.3. Adsorption isotherm models

Table 1 shows the results of Freundlich and Langmuir equilibrium isotherms [93].

According to the results, the R^2 value of the Freundlich model (0.972) was larger than the R^2 value of the Langmuir model (0.952), and the metronidazole adsorption process followed the Freundlich model. In addition, in the Freundlich model, the value of $1/n$ was between zero and one, indicating that the metronidazole adsorption process is favorable. The metronidazole removal by magnetic nanoadsorbents was studied by Asgari et al. [106] and the results revealed that the adsorption process followed the Freundlich isotherm, which was compatible with the findings of this study.

3.4. Kinetic study

Table 2 shows the findings of kinetic investigations of metronidazole adsorption by $CoFe_2O_4$@MC/AC.

Given that the value of R^2 in the pseudo-second-order model (0.999) was greater than the value of R^2 in the pseudo-first-order model (0.289), the pseudo-second-order model explains the adsorption behavior of metronidazole on nanoadsorbents is more appropriate, and the adsorption process of metronidazole by $CoFe_2O_4$@MC/AC followed the pseudo-second-order kinetic model. Asgari et al. [106] kinetic's study of metronidazole adsorption using Fe_3O_4-chitosan nanoadsorbent revealed that the adsorption process kinetic followed a pseudo-second-order kinetic, which was compatible with the findings of this study.

Table 1
Langmuir and Freundlich isotherm parameters (adsorbent: 2.5 g/L, contact time: 20 min, pH: 3)

Freundlich isotherm			Langmuir isotherm			
R^2	k_f (mg/g)(1/mg)	$1/n$	R^2	R_L	Q_m (mg/g)	K_L (1/mg)
				0.221		
				0.159		
4.49	0.972	0.469	0.952	0.124	15.898	0.341
				0.086		
				0.066		

3.5. Thermodynamic study

Table 3 shows the findings of thermodynamic investigations of the metronidazole adsorption mechanism by $CoFe_2O_4$@MC/AC. The exothermic adsorption process is indicated by negative standard enthalpy changes in the reaction.

The values of standard enthalpy changes (ΔH) and standard entropy changes (ΔS) can be obtained by plotting the pick-up diagram $\ln K_d$ vs. $1/T$ (Fig. 8) and deriving the line equation. The Gibbs standard free energy changes (ΔG) can then be calculated at the required temperatures using Eq. (8) [111].

The negative Gibbs energy suggests that the adsorption process is spontaneous, which was compatible with Nasseh et al. [112] investigation on the adsorption of the antibiotic

Table 2
Coefficients for the adsorption kinetics models (MNZ: 10 mg/L, adsorbent: 2.5 g/L, pH = 3)

Pseudo-first-order kinetic model			Pseudo-second-order kinetic model		
R^2	K_1 (min^{-1})	q_e (mg/g)	R^2	K_2 (g/mg·min)	q_e (mg/g)
0.289	0.0817	0.083	0.999	1.73	3.6523

Table 3
Values of thermodynamic parameters of metronidazole adsorption onto $CoFe_2O_4$@MC/AC

T (K)	$\Delta G°$ (kJ/mol)	$\Delta H°$ (kJ/mol)	$\Delta S°$ (J/mol·K)
298	–4.16		
303	–3.45		
308	–3.17	–19.82	–53.57
313	–2.75		
333	–2.15		

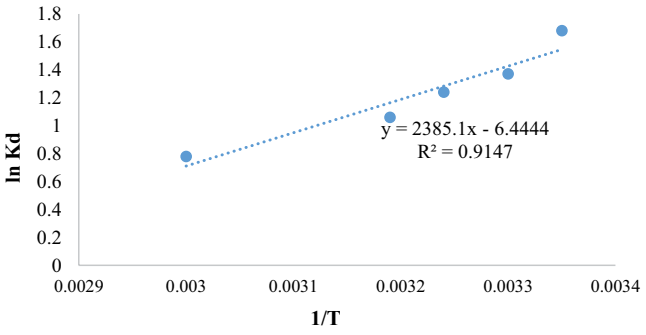

Fig. 8. Van't Hoff plot (pH = 3, dosage nanoadsorbent = 2.5 g/L, concentration MNZ = 10 mg/L).

metronidazole utilizing a novel magnetic nanocomposite derived from simulated wastewater. Negative standard enthalpy changes in the adsorption process imply that it is exothermic, while negative standard entropy changes indicate that the adsorption process is becoming less irregular. The standard entropy changes of the process were negative and demonstrated a reduction in process irregularities in Sun et al. [113] work on the adsorption of metronidazole by sugarcane-derived biochar, which was compatible with the results of this investigation.

3.6. Efficiency of process on real wastewater

The metronidazole adsorption process was carried out on Kerman University of Medical Sciences' real wastewater sample under optimal conditions (pH = 3, nanoadsorbent dose = 2.5 g/L, time = 20 min, temperature = 25°C, MNZ concentration = 10 mg/L). Table 4 shows the results of the physio-chemical quality of this effluent.

In the real sample, the maximum adsorption efficiency was 85%. The efficiency decrease in the real sample is due to the existence of interfering components in the wastewater sample, such as anions and cations, which hinder metronidazole from adsorbing on the adsorbent surface and compete with metronidazole for adsorption on the adsorbent surface [114].

Table 4
Physico-chemical characteristics of real wastewater samples

Amount	Parameters
7.38	pH
143.5	SO_4 (mg/L)
8.0	BOD (mg/L)
26.1	COD (mg/L)
78	TSS (mg/L)
1,194	TDS (mg/L)
1.40	N(NH_3) (mg/L)
1.82	TKN (mg/L)
38.38	PO_4 Orto (mg/L)
10	Metronidazole (mg/L)

3.7. Comparison of $CoFe_2O_4$@MC/AC efficiency with other adsorbents

In Table 5, the efficiency of the $CoFe_2O_4$@MC/AC magnetic nanocomposite in removing pharmaceuticals was compared to that of other synthesized magnetic adsorbents.

The $CoFe_2O_4$@MC/AC magnetic nanocomposite showed a greater removal efficiency in less time, according to Table 5. After four cycles of recovery and reuse, the removal efficiency was 66%. In addition, its efficiency of 85% for real wastewater samples demonstrates the high efficiency of this magnetic nanocomposite in contrast to other synthesized adsorbents.

3.8. Investigation of reusability and stability of $CoFe_2O_4$@MC/AC

Regeneration and reusability of the adsorbent are critical in the adsorption process, both economically and ecologically. Due to its high magnetic strength, the $CoFe_2O_4$@MC/AC magnetic nanocomposite is readily removed from the process environment by a magnet and does not cause secondary contamination in the environment. The removal efficiency of the $CoFe_2O_4$@MC/AC magnetic nanocomposite was 93% in the first cycle and fell to 82% in the second cycle. The contaminant's occupation of adsorbent sites could be the cause of this decrease in efficiency. The chemical stability of the adsorbent was further studied using XRD and FESEM analyses after four times of regeneration and reuse (Fig. 9). The crystal structure and morphology of the nanoadsorbent were still preserved after four steps of regeneration and reuse, according to XRD and FESEM findings, and it can be utilized frequently for the treatment of metronidazole-containing wastewater [25,26,43].

3.9. Adsorption mechanism

The FTIR spectra of the adsorbent were studied before and after the adsorption process to investigate the mechanism of metronidazole adsorption (Fig. 10a). The strength of several peaks in the FTIR spectrum of the adsorbent after the adsorption process reduced or shifted to a lower wavelength, indicating that these functional groups were engaged in the metronidazole adsorption process. As can be seen, the adsorption bands in the 3,450 cm^{-1} are related

Table 5
Comparison of $CoFe_2O_4$@MC/AC with other adsorbents

No.	Adsorbent	Pollutant	Dose of adsorbent (g/L)	Concentration (mg/L)	Contact time (min)	Efficiency (%)		Recovery (%)	Absorption capacity (mg/g)	Ref.
						Synthetic sample	Real sample			
1	Fe_3O_4-Chitosan	Metronidazole	2	10	90	99.05	–	–	–	[88]
2	Biochar derived from sugarcane bagasse	Metronidazole	4	10	120	88.8	–	–	23.61	[91]
3	Rice husk	Metronidazole	3	100	90	90	–	–	–	[122]
4	Biochar rice bran	Metronidazole	1.5	10	45	90	–	–	21.33	[123]
5	$CoFe_2O_4$@MC/AC	Metronidazole	2	10	20	93	85	66% 4 cycles	15.90	This work

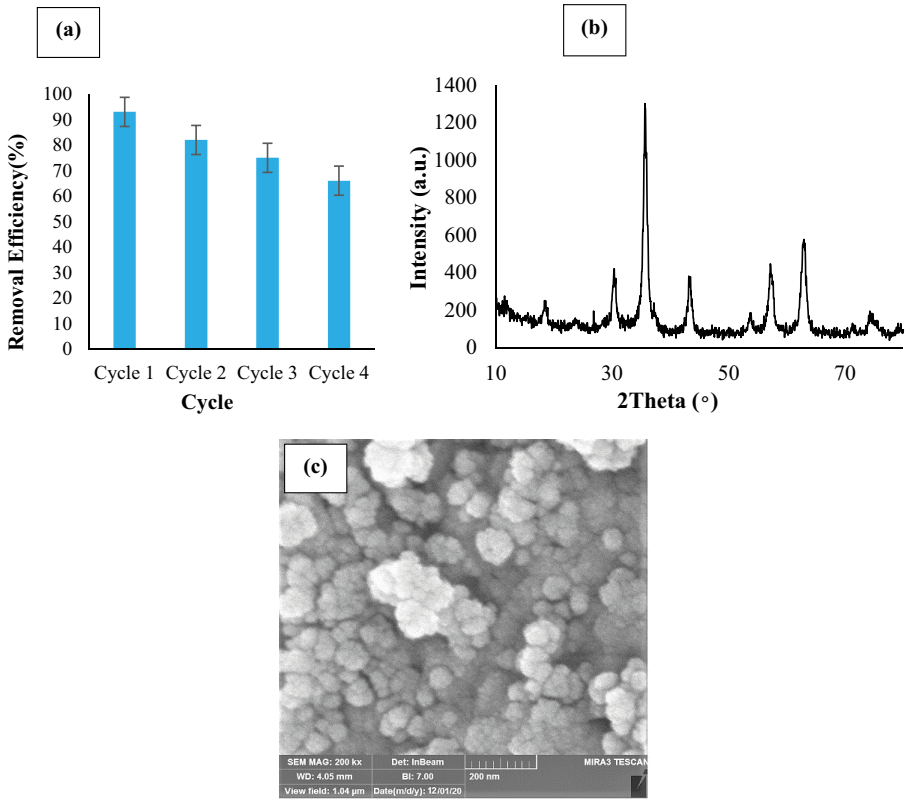

Fig. 9. Recycling of $CoFe_2O_4$@MC/AC in the removal of metronidazole (a), XRD (b), and FESEM (c) analysis after four recovery steps.

to the tensile vibrations of the hydroxyl functional groups, the adsorption band in the 1,600 cm^{-1} is related to the tensile vibrations of the dual bands C=C, and the adsorption band in the 1,081 cm^{-1} is related to the tensile vibrations of the bands C–O–C have decreased in intensity and shifted to lower wavelengths, demonstrating that these groups are involved in the metronidazole adsorption process. Also, the possible mechanisms for metronidazole adsorption by $CoFe_2O_4$@MC/AC are shown in Fig. 10b. The additional interactions may be implicated in the metronidazole adsorption step through the electrostatic attraction between metronidazole and the adsorbent. The π-electron of the metronidazole molecule's heterocyclic aromatic ring, on the other hand, would interact with distinct $CoFe_2O_4$@MC/AC sites. Methylcellulose is a polymer made mostly of polysaccharides that is highly hydrated. The foundation of MC is a highly hydrophilic polymer and long-chain polysaccharide comprising glucose monomers that are joined together by beta bonds. The polysaccharide CH group forms a CH-π bond with the π-electrons of aromatic molecules [115,116]. As a result, metronidazole molecule adsorption in the scaffold of the polysaccharide matrix would require a van der Waals attraction between the π-electron of the heterocyclic aromatic ring of the metronidazole molecule and the hydrogen atom of the CH group of the MC to generate a CH-π bond. Another mechanism might be an OH-π bond with the Hydroxyl group of MC. $CoFe_2O_4$@MC/AC, on the other hand, has a complicated structure in which the OH groups of MC engaged in intermolecular interactions may be depleted of free OH to form bonds with metronidazole [115]. Saccharides are polar, however, due to the direction of OH groups, which have a preference for forming hydrogen bonds with hydrophobic compounds, they may include some hydrophobic constituents [115,117]. Metronidazole's hydrophobic imidazole ring would generate an OH-π bond with hydrophobic moieties' OH groups. Metronidazole interacts with its π electron to generate π–π dispersion bonds with other molecules, according to previous research [118]. $CoFe_2O_4$@MC/AC magnetic adsorbent with AC with π electron would be predicted to facilitate the development of π–π dispersion bonds for metronidazole interaction. Metronidazole's alkyl side chain also contributes to the adsorbent's binding [119]. Additionally, the $CoFe_2O_4$@MC/AC magnetic adsorbent was included functional groups such as hydroxyl and methoxy groups that may form H-bonds with metronidazole.

3.10. Performance comparison of $CoFe_2O_4$@MC/AC, AC, and $CoFe_2O_4$

Fig. 11 compares the metronidazole adsorption efficiencies of activated carbon, $CoFe_2O_4$, and the $CoFe_2O_4$@MC/AC nanocomposite under optimum adsorption circumstances. The results revealed that activated carbon, which has a higher adsorption capacity than $CoFe_2O_4$@MC/AC and $CoFe_2O_4$, had a better removal efficiency than the other two adsorbents. However, its separation and regeneration require more time, cost, and energy than those of the other two adsorbents. Due to the lack of active carbon and methyl cellulose in its structure, the $CoFe_2O_4$ adsorbent

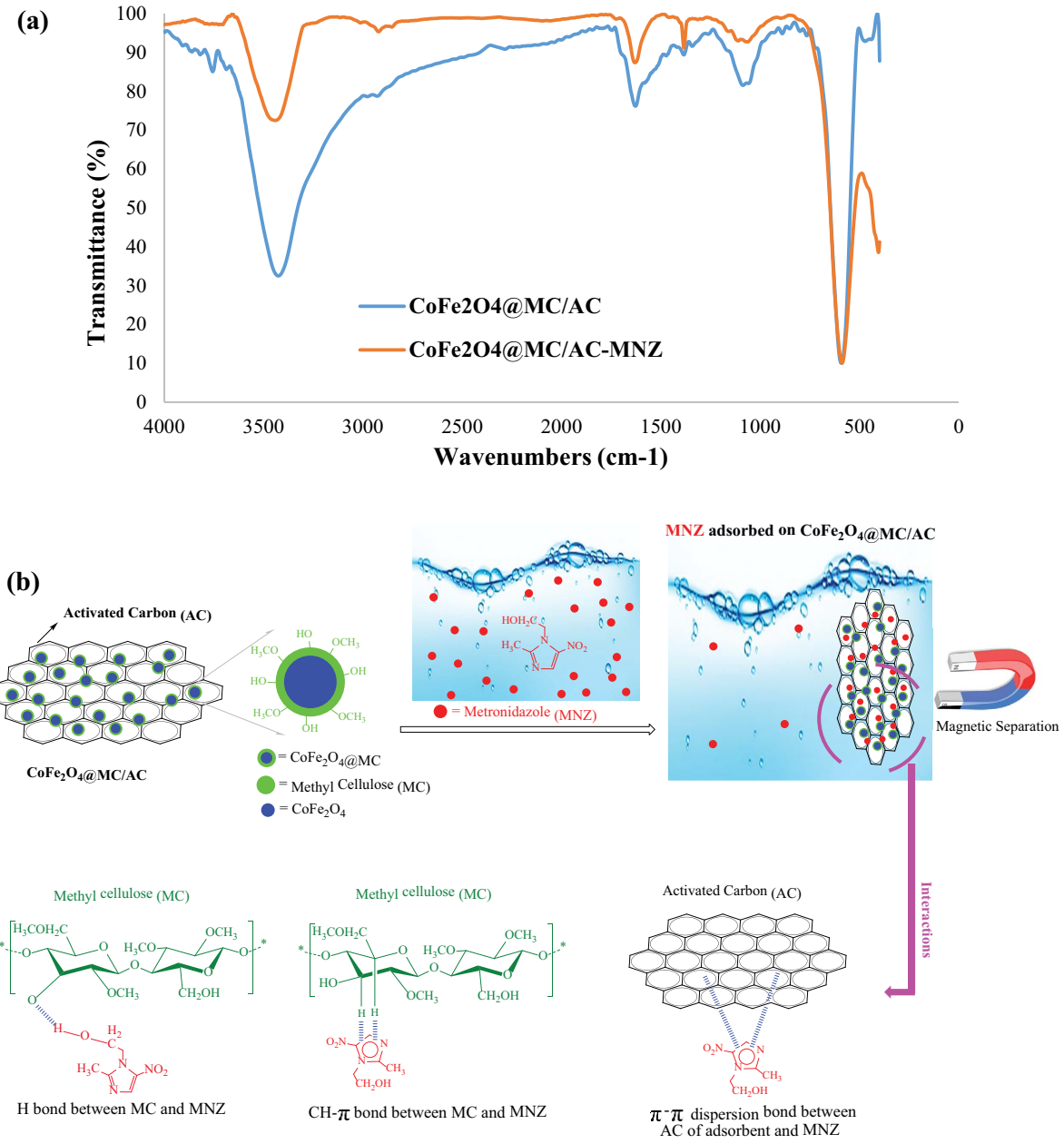

Fig. 10. FTIR of $CoFe_2O_4$@MC/AC before and after metronidazole adsorption (a) and mechanism of metronidazole adsorption.

was less effective in removing metronidazole than the other two adsorbents. The adsorbent's effectiveness in adsorbing metronidazole is increased by the high capacity of activated carbon for adsorption and the existence of functional groups in methylcellulose in its structural composition [48]. Because active carbon and methylcellulose were included in the structure of the produced $CoFe_2O_4$@MC/AC nanocomposite, it exhibited a better removal efficiency than cobalt ferrite.

4. Toxicity assay through Artemia and Daphnia

In accordance with the OECD Guideline (2014) on evaluating the environmental destiny of nanomaterials in aquatic environments, and given that, before this study, very limited information was only known on the possible risk assessment of chemical magnetite nanoparticles in organisms like *Artemia* and *Daphnia*, these animals have a very significant place in the pyramid of matter and energy in aquatic food chains as models of nano-ecological animals and even higher levels of food chains can act as representatives of the secondary consumer group and can act as transmitter nanoparticles [120]. As a result, the acute toxicity of $CoFe_2O_4$@MC/AC nanoparticles in saline and freshwater aquatic species was assessed and compared in this study. Table 6 shows the results of toxicity studies of synthetic effluent samples on *Artemia* and *Daphnia* aquifers under optimal conditions. Toxicity was assessed on a synthetic effluent sample of 10 to 100 vol.% (10%, 25%, 50%, 75%, and 100%) and a

Table 6
Determination of LC_{50} value and toxicity unit (TU) of effluent by *Artemia* and *Daphnia*

Desired criteria (95% confidence)	12 h		24 h		36 h		48 h		72 h	
	Artemia	*Daphnia*	*Artemia*	*Daphnia*	*Artemia*	*Daphnia*	*Artemia*	*Daphnia*	*Artemia*	*Daphnia*
LC_{50} (mg/L)	224.073	166.37	181.118	212.398	172.383	185.580	157.984	181.458	152.598	173.201
LC_{50} max. (mg/L)	4,277.165	587.738	522.673	1560	439.514	844.562	335.278	1,303.393	310.876	988.821
LC_{50} min. (mg/L)	140.175	122.461	126.083	134.7	122.167	120.731	115.337	114.626	111.967	110.952
TU (toxicity unit)	0.446	0.601	0.552	0.470	0.580	0.539	0.633	0.551	0.655	0.577

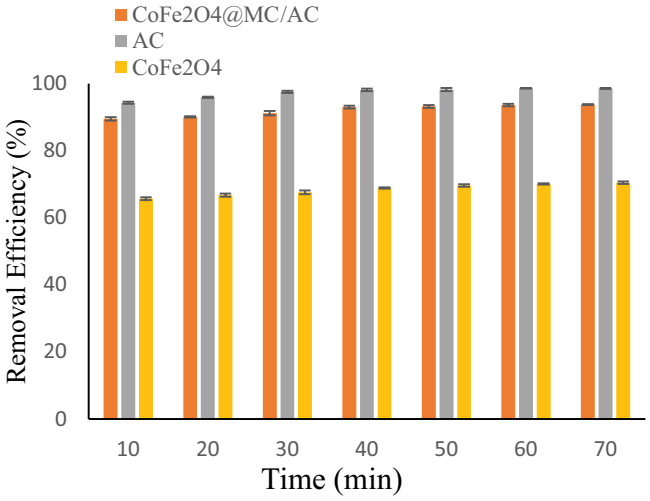

Fig. 11. The performance comparison of $CoFe_2O_4$@MC/AC, AC, and $CoFe_2O_4$ for metronidazole adsorption (temperature = 25°C, pH = 3, dosage nanoadsorbent = 2.5 g/L, concentration MNZ = 10 mg/L).

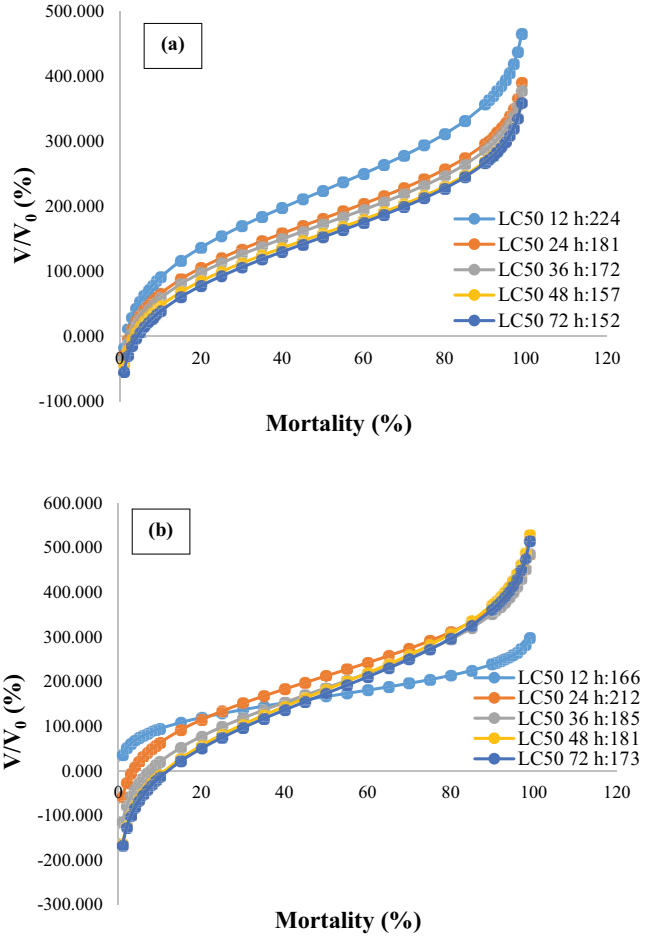

Fig. 12. *Artemia* (a) and *Daphnia* (b) mortality at different times and concentrations of effluent.

control sample with three repeats. Given that there were 30 *Artemia* and *Daphnia* in each sample container at the beginning, the number of dead *Artemia* and *Daphnia* was counted after 12, 24, 36, 48, and 72 h. The LC_{50} of the samples, as well as the toxicity unit (TU), were then calculated using SPSS software probit analysis [88,121]. *Artemia* and *Daphnia* might both die at varying doses of metronidazole, as seen in Fig. 12a and b. The effects of effluent toxicity on *Daphnia* and *Artemia* have risen with increasing concentration and also with increasing exposure time, as shown in Table 6. However, the death rate for *Daphnia* and *Artemia* after 72 h. at the maximum effluent concentration (100% by volume) was 33.3% for *Daphnia* and 26.6% for *Artemia*, according to the findings. The toxicity of the effluent following the adsorption process was found to be minimal under optimal conditions, indicating that it was not detrimental to the environment.

5. Conclusion

The magnetic nanocomposite $CoFe_2O_4$@MC/AC was synthesized utilizing a rapid green method in the presence of methylcellulose biopolymers and activated carbon in this study. BET, VSM, XRD, FESEM, EDS, FTIR, and mapping & Line scan techniques were used to structurally evaluate the synthesized magnetic nanocomposites. The structural study revealed that the nano-scale nanoadsorbent was synthesized as homogeneous spherical nanoparticles with no lumps, high magnetic strength (57.91 emu/g), high surface area (128.22 m^2/g), and strong heat resistance while preserving the crystal structure. The removal efficiency of metronidazole by this magnetic nanocomposite in synthetic and real wastewater samples was 93% and 85%, respectively, under optimal conditions of pH = 3, nanoadsorbent dose = 2.5 g/L, contact time = 20 min, temperature = 25°C, and MNZ initial concentration = 10 mg/L. The adsorption mechanism for metronidazole was consistent with a pseudo-second-order

kinetic and Freundlich isotherm, according to adsorption kinetics and isotherms. Metronidazole adsorption was an exothermic process. The synthesized magnetic nanocomposite could also regenerate and reuse, and had a removal efficiency of 66% of metronidazole from the aqueous solution after four cycles of regeneration and reuse. The toxicity effects of *Daphnia* and *Artemia* effluents increased with increasing concentration and also with increasing effluent exposure time, according to the LC_{50} values. However, the death rate for *Daphnia* and *Artemia* after 72 h at the maximum effluent concentration (100% by volume) was 33.3% for *Daphnia* and 26.6% for *Artemia*, according to the findings. These findings indicated that this magnetic nanocomposite can be utilized to eliminate metronidazole from water polluted with contaminants and might be employed in the pharmaceutical industries for wastewater treatment.

Acknowledgments

This research is the result of a master's thesis in environmental toxicology with project number 400000417 and IR.KMU.REC.1400.376 ethic approval cod. It was conducted in the Environmental Health Engineering Research Center of Kerman University of Medical Sciences. This research was supported by the Vice-Chancellor for Research and Technology of Kerman University of Medical Sciences.

Author statement

Najmeh Golestani: Investigation, methodology, writing the original draft. Alireza Nasiri: Advisor, writing-reviewing and editing, software, visualization, validation. Majid Hashemi: Supervision, writing-reviewing and editing, visualization, validation.

References

[1] S. Rajabi, A. Nasiri, M. Hashemi, Enhanced activation of persulfate by $CuCoFe_2O_4$@MC/AC as a novel nanomagnetic heterogeneous catalyst with ultrasonic for metronidazole degradation, Chemosphere, 286 (2022) 131872, doi: 10.1016/j.chemosphere.2021.131872.

[2] N. Aarab, A. Hsini, A. Essekri, M. Laabd, R. Lakhmiri, A. Albourine, Removal of an emerging pharmaceutical pollutant (metronidazole) using PPY-PANi copolymer: kinetics, equilibrium and DFT identification of adsorption mechanism, Groundwater Sustainable Dev., 11) 2020) 100416, doi: 10.1016/j.gsd.2020.100416.

[3] Z. Derakhshan, M. Mokhtari, F. Babaei, R. Malek Ahmadi, M.H. Ehrampoush, M. Faramarzian, Removal methods of antibiotic compounds from aqueous environments–a review, J. Environ. Health Sustainable Dev., 1 (2016) 51–74.

[4] M.J. Ahmed, S.K. Theydan, Microwave assisted preparation of microporous activated carbon from *Siris* seed pods for adsorption of metronidazole antibiotic, Chem. Eng. J., 214 (2013) 310–318.

[5] M. Malakootian, K. Kannan, M.A. Gharaghani, A. Dehdarirad, A. Nasiri, Y.D. Shahamat, H. Mahdizadeh, Removal of metronidazole from wastewater by Fe/charcoal micro electrolysis fluidized bed reactor, J. Environ. Chem. Eng., 7 (2019) 103457, doi: 10.1016/j.jece.2019.103457.

[6] F. Mohammadi, Z. Yavari, S. Rahimi, M. Hashemi, Artificial neural network modeling of Cr(VI) biosorption from aqueous solutions, J. Water Chem. Technol., 41 (2019) 219–227.

[7] R.F. Dantas, O. Rossiter, A.K.R. Teixeira, A.S.M. Simões, V.L. da Silva, Direct UV photolysis of propranolol and metronidazole in aqueous solution, Chem. Eng. J., 158 (2010) 143–147.

[8] M. Malakootian, M. Hashemi, A. Toolabi, A. Nasiri, Investigation of nickel removal using poly(amidoamine) generation 4 dendrimer (PAMAM G4) from aqueous solutions, J. Eng. Res., 6 (2018) 13–23.

[9] A. Pasgar, A. Nasiri, N. Javid, Single and competitive adsorption of Cu^{2+} and Pb^{2+} by tea pulp from aqueous solutions, Environ. Health Eng. Manage. J., 9 (2022) 65–74.

[10] M. Malakootian, A. Nasiri, M.R. Heidari, Removal of phenol from steel plant wastewater in three dimensional electrochemical (TDE) process using $CoFe_2O_4$@AC/H_2O_2, Z. Phys. Chem., 234 (2020) 1661–1679.

[11] Z. Fang, J. Chen, X. Qiu, X. Qiu, W. Cheng, L. Zhu, Effective removal of antibiotic metronidazole from water by nanoscale zero-valent iron particles, Desalination, 268 (2011) 60–67.

[12] H. Wang, G. Zhang, Y. Gao, Photocatalytic degradation of metronidazole in aqueous solution by niobate $K_6Nb_{10.8}O_{30}$, Wuhan Univ. J. Nat. Sci., 15 (2010) 345–349.

[13] N. Okhovat, M. Hashemi, A.A. Golpayegani, Photocatalytic decomposition of Metronidazolein aqueous solutions using titanium dioxide nanoparticles, J. Mater. Environ. Sci., 6 (2015) 792–799.

[14] C. Wang, R. Huang, R. Sun, J. Yang, M. Sillanpää, A review on persulfates activation by functional biochar for organic contaminants removal: synthesis, characterizations, radical determination, and mechanism, J. Environ. Chem. Eng., 9 (2021) 106267, doi: 10.1016/j.jece.2021.106267.

[15] C. Wang, R. Sun, R. Huang, H. Wang, Superior Fenton-like degradation of tetracycline by iron loaded graphitic carbon derived from microplastics: synthesis, catalytic performance, and mechanism, Sep. Purif. Technol., 270 (2021) 118773, doi: 10.1016/j.seppur.2021.118773.

[16] R. Huang, J. Yang, Y. Cao, D.D. Dionysiou, C. Wang, Peroxymonosulfate catalytic degradation of persistent organic pollutants by engineered catalyst of self-doped iron/carbon nanocomposite derived from waste toner powder, Sep. Purif. Technol., 291 (2022) 120963, doi: 10.1016/j.seppur.2022.120963.

[17] M. Malakootian, J. Smith, M. Gharaghani, H. Mahdizadeh, A. Nasiri, G. Yazdanpanah, Decoloration of textile Acid Red 18 dye by hybrid UV/COP advanced oxidation process using ZnO as a catalyst immobilized on a stone surface, Desal. Water Treat., 182 (2020) 385–394.

[18] A. Babuponnusami, K. Muthukumar, A review on Fenton and improvements to the Fenton process for wastewater treatment, J. Environ. Chem. Eng., 2 (2014) 557–572.

[19] M. Umar, H.A. Aziz, M.S. Yusoff, Trends in the use of Fenton, electro-Fenton and photo-Fenton for the treatment of landfill leachate, Waste Manage., 30 (2010) 2113–2121.

[20] N. Sharifi, A. Nasiri, S.S. Martínez, H. Amiri, Synthesis of Fe_3O_4@activated carbon to treat metronidazole effluents by adsorption and heterogeneous Fenton with effluent bioassay, J. Photochem. Photobiol., A, 427 (2022) 113845, doi: 10.1016/j.jphotochem.2022.113845.

[21] D. Martínez-Pachón, M. Ibáñez, F. Hernández, R.A. Torres-Palma, A. Moncayo-Lasso, Photo-electro-Fenton process applied to the degradation of valsartan: effect of parameters, identification of degradation routes and mineralization in combination with a biological system, J. Environ. Chem. Eng., 6 (2018) 7302–7311.

[22] H. Dastpak, H. Pasalari, A.J. Jafari, M. Gholami, M. Farzadkia, Improvement of Co-composting by a combined pretreatment ozonation/ultrasonic process in stabilization of raw activated sludge, Sci. Rep., 10 (2020) 1070, doi: 10.1038/s41598-020-58054-y

[23] F. Deng, S. Qiu, C. Chen, X. Ding, F. Ma, Heterogeneous catalytic ozonation of refinery wastewater over alumina-supported Mn and Cu oxides catalyst, Ozone: Sci. Eng., 37 (2015) 546–555.

[24] H. Mahdizadeh, A. Nasiri, M.A. Gharaghani, G. Yazdanpanah, Hybrid UV/COP advanced oxidation process using ZnO as a catalyst immobilized on a stone surface for degradation of acid red 18 dye, MethodsX, 7 (2020) 101118, doi: 10.1016/j.mex.2020.101118.

[25] M. Malakootian, A. Nasiri, A. Asadipour, M. Faraji, E. Kargar, A facile and green method for synthesis of $ZnFe_2O_4$@CMC as

a new magnetic nanophotocatalyst for ciprofloxacin removal from aqueous media, MethodsX, 6 (2019) 1575–1580.
[26] M. Malakootian, A. Nasiri, H. Mahdizadeh, Metronidazole adsorption on $CoFe_2O_4$/activated carbon@chitosan as a new magnetic biocomposite: modelling, analysis, and optimization by response surface methodology, Desal. Water Treat., 164 (2019) 215–227.
[27] M. Malakootian, J.A. Smith, M.A. Gharaghani, H. Mahdizadeh, A. Nasiri, G. Yazdanpanah, Decoloration of textile Acid Red 18 dye by hybrid UV/COP advanced oxidation process using ZnO as a catalyst immobilized on a stone surface, Desal. Water Treat., 18 (2020) 385–394.
[28] A. Chavoshani, M.M. Amin, G. Asgari, A. Seidmohammadi, M. Hashemi, Chapter 8 – Microwave/Hydrogen Peroxide Processes, S.C. Ameta, R. Ameta, Eds., Advanced Oxidation Processes for Waste Water Treatment, Academic Press, Amsterdam, 2018, pp. 215–255.
[29] M. Malakootian, A. Nasiri, M. Khatami, H. Mahdizadeh, P. Karimi, M. Ahmadian, N. Asadzadeh, M.R. Heidari, Experimental data on the removal of phenol by electro-H_2O_2 in presence of UV with response surface methodology, MethodsX, 6 (2019) 1188–1193.
[30] M. Malakootian, N. Olama, M. Malakootian, A. Nasiri, Photocatalytic degradation of metronidazole from aquatic solution by TiO_2-doped Fe^{3+} nano-photocatalyst, Int. J. Environ. Sci. Technol., 16 (2019) 4275–4284.
[31] G. Zolfaghari, M. Kargar, Nanofiltration and microfiltration for the removal of chromium, total dissolved solids, and sulfate from water, MethodsX, 6 (2019) 549–557.
[32] M.R. Muthumareeswaran, M. Alhoshan, G.P. Agarwal, Ultrafiltration membrane for effective removal of chromium ions from potable water, Sci. Rep., 7 (2017) 41423, doi: 10.1038/srep41423.
[33] B. Karimi, S. Khanaki, L. Ma'mani, S.M. Khezri, A. Karami, Efficient removal of organophosphate pesticide imidacloprid from water samples by modified magnetic-silica core-shell nanoparticles as a recoverable nanoadsorbent, J. School Public Health Inst. Public Health Res., 15 (2018) 389–400.
[34] Y. Wang, C. Shen, M. Zhang, B.-T. Zhang, Y.-G. Yu, The electrochemical degradation of ciprofloxacin using a SnO_2-Sb/Ti anode: influencing factors, reaction pathways and energy demand, Chem. Eng. J., 296 (2016) 79–89.
[35] M. Malakootian, A. Nasiri, M.R. Heidari, Removal of phenol from steel plant wastewater in three dimensional electrochemical (TDE) process using $CoFe_2O_4$@AC/H_2O_2, Z. Phys. Chem., 234 (2019) 1661–1679.
[36] R. Nodehi, K.A. Rahbar, Removal of amoxicillin from an aqueous medium with the modified natural zeolite, J. Appl. Res. Chem., 13 (2020) 127–138.
[37] S. Sadeghi, G. Raki, A. Amini, N. Mengelizadeh, M.M. Amin, M. Hashemi, Study of the effectiveness of the third generation polyamideamine and polypropylene imine dendrimers in removal of reactive blue 19 dye from aqueous solutions, Environ. Health Eng. Manage., 5 (2018) 197–203.
[38] K. Adibkia, M. Barzegar-Jalali, Y. Javadzadeh, R. Bayrami, G. Mohammadi, A review on the porous adsorbents in drug delivery systems, J. Pharm. Sci., 18 (2012) 103–118.
[39] A. Nasiri, S. Rajabi, M. Hashemi, H. Nasab, $CuCoFe_2O_4$@MC/AC as a new hybrid magnetic nanocomposite for metronidazole removal from wastewater: bioassay and toxicity of effluent, Sep. Purif. Technol., (2022) 121366.
[40] N. Ballav, H.J. Choi, S.B. Mishra, A. Maity, Synthesis, characterization of Fe_3O_4@glycine doped polypyrrole magnetic nanocomposites and their potential performance to remove toxic Cr(VI), J. Ind. Eng. Chem., 20 (2014) 4085–4093.
[41] N. Javid, A. Nasiri, M. Malakootian, Removal of nonylphenol from aqueous solutions using carbonized date pits modified with ZnO nanoparticles, Desal. Water Treat., 141 (2019) 140–148.
[42] A. Nasiri, M. Malakootian, M.R. Heidari, S.N. Asadzadeh, $CoFe_2O_4$@methylcelloluse as a new magnetic nano biocomposite for sonocatalytic degradation of Reactive Blue 19, J. Polym. Environ., 29 (2021) 2660–2675.
[43] A. Nasiri, M. Malakootian, M.A. Shiri, G. Yazdanpanah, M. Nozari, $CoFe_2O_4$@methylcellulose synthesized as a new magnetic nanocomposite to tetracycline adsorption: modeling, analysis, and optimization by response surface methodology, J. Polym. Res., 28 (2021) 192, doi: 10.1007/s10965-021-02540-y.
[44] S.C. Goh, C.H. Chia, S. Zakaria, M. Yusoff, C.Y. Haw, S. Ahmadi, N.M. Huang, H.N. Lim, Hydrothermal preparation of high saturation magnetization and coercivity cobalt ferrite nanocrystals without subsequent calcination, Mater. Chem. Phys., 120 (2010) 31–35.
[45] M. Malakootian, M. Khatami, H. Mahdizadeh, A. Nasiri, M. Amiri Gharaghani, A study on the photocatalytic degradation of p-Nitroaniline on glass plates by thermo-immobilized ZnO nanoparticle, Inorg. Nano-Metal Chem., 50 (2019) 124–135.
[46] H. Pourzamani, M. Hashemi, B. Bina, A. Rashidi, M.M. Amin, S. Parastar, Toluene removal from aqueous solutions using single-wall carbon nanotube and magnetic nanoparticle–hybrid adsorbent, J. Environ. Eng., 144 (2018) 04017104, doi: 10.1061/(ASCE)EE.1943-7870.0001318.
[47] S. Fadaei, F.N. Moghadam, M. Hashemi, H. Pourzamani, BTEX removal from aqueous solution by modified multi-walled carbon nanotubes with ozone, Anuário do Instituto de Geociências – UFRJ, 40 (2017) 235–242.
[48] A. Nasiri, S. Rajabi, M. Hashemi, $CoFe_2O_4$@methylcellulose/AC as a new, green, and eco-friendly nano-magnetic adsorbent for removal of Reactive Red 198 from aqueous solution, Arabian J. Chem., 15 (2022) 103745.
[49] A. Nasiri, S. Rajabi, A. Amiri, M. Fattahizade, O. Hasani, A. Lalehzari, M. Hashemi, Adsorption of tetracycline using $CuCoFe_2O_4$@chitosan as a new and green magnetic nanohybrid adsorbent from aqueous solutions: isotherm, kinetic and thermodynamic study, Arabian J. Chem., 15 (2022) 104014, doi: 10.1016/j.arabjc.2022.104014.
[50] A. Nasiri, M. Malakootian, N. Javid, Modelling and optimization of lead adsorption by $CoFe_2O_4$@CMC@HZSM-5 from aqueous solution using response surface methodology, Desal. Water Treat., 248 (2022) 134–148.
[51] A. Nasiri, M. Malakootian, M.A. Shiri, G. Yazdanpanah, M. Nozari, $CoFe_2O_4$@methylcellulose synthesized as a new magnetic nanocomposite to tetracycline adsorption: modeling, analysis, and optimization by response surface methodology, J. Polym. Res., 28 (2021) 1–23.
[52] J.Rivera-Utrilla,C.V.Gómez-Pacheco,M.Sánchez-Polo,J.J.López-Peñalver, R Ocampo-Pérez, Tetracycline removal from water by adsorption/bioadsorption on activated carbons and sludge-derived adsorbents, J. Environ. Manage., 131 (2013) 16–24.
[53] F. Marrakchi, M. Ahmed, W. Khanday, M. Asif, B. Hameed, Mesoporous-activated carbon prepared from chitosan flakes via single-step sodium hydroxide activation for the adsorption of methylene blue, Int. J. Biol. Macromol., 98 (2017) 233–239.
[54] W. Khanday, F. Marrakchi, M. Asif, B. Hameed, Mesoporous zeolite–activated carbon composite from oil palm ash as an effective adsorbent for methylene blue, J. Taiwan Inst. Chem. Eng., 70 (2017) 32–41.
[55] M.A. Islam, M. Ahmed, W. Khanday, M. Asif, B. Hameed, Mesoporous activated carbon prepared from NaOH activation of rattan (*Lacosperma secundiflorum*) hydrochar for methylene blue removal, Ecotoxicol. Environ. Saf., 138 (2017) 279–285.
[56] M.A. Islam, S. Sabar, A. Benhouria, W. Khanday, M. Asif, B. Hameed, Nanoporous activated carbon prepared from karanj (*Pongamia pinnata*) fruit hulls for methylene blue adsorption, J. Taiwan Inst. Chem. Eng., 74 (2017) 96–104.
[57] F. Marrakchi, W. Khanday, M. Asif, B. Hameed, Cross-linked chitosan/sepiolite composite for the adsorption of methylene blue and reactive orange 16, Int. J. Biol. Macromol., 93 (2016) 1231–1239.
[58] W. Khanday, M. Asif, B. Hameed, Cross-linked beads of activated oil palm ash zeolite/chitosan composite as a bio-adsorbent for the removal of methylene blue and acid blue 29 dyes, Int. J. Biol. Macromol., 95 (2017) 895–902.
[59] D. Yuan, J. Ding, J. Zhou, L. Wang, H. Wan, W.-L. Dai, G. Guan, Graphite carbon nitride nanosheets decorated with ZIF-8

nanoparticles: effects of the preparation method and their special hybrid structures on the photocatalytic performance, J. Alloys Compd., 762 (2018) 98–108.
[60] Q.-Q. Zhang, G.-G. Ying, C.-G. Pan, Y.-S. Liu, J.-L. Zhao, Comprehensive evaluation of antibiotics emission and fate in the river basins of China: source analysis, multimedia modeling, and linkage to bacterial resistance, Environ. Sci. Technol., 49 (2015) 6772–6782.
[61] P. Liu, W.-J. Liu, H. Jiang, J.-J. Chen, W.-W. Li, H.-Q. Yu, Modification of bio-char derived from fast pyrolysis of biomass and its application in removal of tetracycline from aqueous solution, Bioresour. Technol., 121 (2012) 235–240.
[62] M. Ghaedi, S. Hajjati, Z. Mahmudi, I. Tyagi, S. Agarwal, A Maity, V.K. Gupta, Modeling of competitive ultrasonic assisted removal of the dyes – Methylene blue and Safranin-O using Fe_3O_4 nanoparticles, Chem. Eng. J., 268 (2015) 28–37.
[63] N. Amirmahani, N.O. Mahmoodi, M. Bahramnejad, N. Seyedi, Recent developments of metallic nanoparticles and their catalytic activity in organic reactions, J. Chin. Chem. Soc., 67 (2020) 1326–1337.
[64] H. Pourzamani, S. Parastar, M. Hashemi, The elimination of xylene from aqueous solutions using single wall carbon nanotube and magnetic nanoparticle hybrid adsorbent, Process Saf. Environ. Prot., 109 (2017) 688–696.
[65] K. Ventura, R.A. Arrieta, M. Marcos-Hernández, V. Jabbari, C.D.Powell,R.Turley,A.W.Lounsbury,J.B.Zimmerman,J.Gardea-Torresdey, M.S. Wong, D. Villagrán, Superparamagnetic MOF@GO Ni and Co based hybrid nanocomposites as efficient water pollutant adsorbents, Sci. Total Environ., 738 (2020) 139213, doi: 10.1016/j.scitotenv.2020.139213.
[66] A. Benvidi, M. Yekrangi, S. Jahanbani, H.R. Zare, The extraction and measurement of nickel metal ion in crab, shellfish and rice samples using magnetic silk fibroin – EDTA ligand and furnace atomic absorption spectrometry, Food Chem., 319 (2020) 126432, doi: 10.1016/j.foodchem.2020.126432.
[67] H.A.L. de Oliveira, A.F.C. Campos, G. Gomide, Y. Zhang, S. Ghoshal, Elaboration of a core@shell bimagnetic nanoadsorbent ($CoFe_2O_4$@γ-Fe_2O_3) for the removal of As(V) from water, Colloids Surf., A, 600 (2020) 125002, doi: 10.1016/j.colsurfa.2020.125002.
[68] F. Movahhedi, A. Maghsodi, L. Adlnasab, Response surface methodology for heavy metals removal by tioglycolic-modified Zn–Fe layer double hydroxide as a magnetic recyclable adsorbent, Chem. Pap., 74 (2020) 3169–3182.
[69] A. Ghiasi, A. Malekpour, Octyl coated cobalt-ferrite/silica core-shell nanoparticles for ultrasonic assisted-magnetic solid-phase extraction and speciation of trace amount of chromium in water samples, Microchem. J., 154 (2020) 104530, doi: 10.1016/j.microc.2019.104530.
[70] S.K. Sahoo, S. Padhiari, S.K. Biswal, B.B. Panda, G. Hota, Fe_3O_4 nanoparticles functionalized GO/g-C_3N_4 nanocomposite: an efficient magnetic nanoadsorbent for adsorptive removal of organic pollutants, Mater. Chem. Phys., 244 (2020) 122710, doi: 10.1016/j.matchemphys.2020.122710.
[71] T. Tang, S. Cao, C. Xi, X. Li, L. Zhang, G. Wang, Z. Chen, Chitosan functionalized magnetic graphene oxide nanocomposite for the sensitive and effective determination of alkaloids in hotpot, Int. J. Biol. Macromol., 146 (2020) 343–352.
[72] K.C. Das, B. Das, S.S. Dhar, Effective catalytic degradation of organic dyes by nickel supported on hydroxyapatite-encapsulated cobalt ferrite (Ni/HAP/$CoFe_2O_4$) magnetic novel nanocomposite, Water Air Soil Pollut., 231 (2020) 43, doi: 10.1007/s11270-020-4409-1.
[73] B. D'Cruz, M. Madkour, M.O. Amin, E. Al-Hetlani, Efficient and recoverable magnetic AC-Fe_3O_4 nanocomposite for rapid removal of promazine from wastewater, Mater. Chem. Phys., 240 (2020) 122109, doi: 10.1016/j.matchemphys.2019.122109.
[74] S. Ling, W. Chen, Y. Fan, K. Zheng, K. Jin, H. Yu, M.J. Buehler, D.L. Kaplan, Biopolymer nanofibrils: structure, modeling, preparation, and applications, Prog. Polym. Sci., 85 (2018) 1–56.
[75] S. Nandi, P. Guha, A review on preparation and properties of cellulose nanocrystal-incorporated natural biopolymer, J. Packag. Technol. Res., 2 (2018) 149–166.
[76] M.H. Mehdinejad, N. Mengelizadeh, A. Bay, H. Pourzamani, Y. Hajizadeh, N. Niknam, A.H. Moradi, M. Hashemi, H. Mohammadi, Adsorption of methylene blue from aqueous solutions by cellulose and nanofiber cellulose and its electrochemical regeneration, Desal. Water Treat., 110 (2018) 250–263.
[77] M. Malakootian, A. Nasiri, A. Asadipour, E. Kargar, Facile and green synthesis of $ZnFe_2O_4$@CMC as a new magnetic nano-photocatalyst for ciprofloxacin degradation from aqueous media, Process Saf. Environ. Prot., 129 (2019) 138–151.
[78] M. Malakootian, A. Nasiri, H. Mahdizadeh, Preparation of $CoFe_2O_4$/activated carbon@chitosan as a new magnetic nanobiocomposite for adsorption of ciprofloxacin in aqueous solutions, Water Sci. Technol., 78 (2018) 2158–2170.
[79] A. Nasiri, F. Tamaddon, M.H. Mosslemin, M. Faraji, A microwave assisted method to synthesize nano-$CoFe_2O_4$@methyl cellulose as a novel metal-organic framework for antibiotic degradation, MethodsX, 6 (2019) 1557–1563.
[80] A. Nasiri, F. Tamaddon, M.H. Mosslemin, M.A. Gharaghani, A. Asadipour, New magnetic nanobiocomposite $CoFe_2O_4$@methycellulose: facile synthesis, characterization, and photocatalytic degradation of metronidazole, J. Mater. Sci. - Mater. Electron. 30 (2019) 8595–8610.
[81] M. Malakootian, H. Mahdizadeh, M. Khavari, A. Nasiri, M.A. Gharaghani, M. Khatami, E. Sahle-Demessie, R.S. Varma, Efficiency of novel Fe/charcoal/ultrasonic micro-electrolysis strategy in the removal of Acid Red 18 from aqueous solutions, J. Environ. Chem. Eng., 8 (2020) 103553, doi: 10.1016/j.jece.2019.103553.
[82] F. Tamaddon, M.H. Mosslemin, A. Asadipour, M.A. Gharaghani, A. Nasiri, Microwave-assisted preparation of $ZnFe_2O_4$@methyl cellulose as a new nano-biomagnetic photocatalyst for photodegradation of metronidazole, Int. J. Biol. Macromol., 154 (2020) 1036–1049.
[83] F. Tamaddon, A. Nasiri, G. Yazdanpanah, Photocatalytic degradation of ciprofloxacin using $CuFe_2O_4$@methyl cellulose based magnetic nanobiocomposite, MethodsX, 7 (2020) 100764, doi: 10.1016/j.mex.2019.12.005.
[84] A. Nasiri, M. Malakootian, M.R. Heidari, S.N. Asadzadeh, $CoFe_2O_4$@methylcelloluse as a new magnetic nano biocomposite for sonocatalytic degradation of reactive blue 19, J. Polym. Environ., 29 (2021) 2660–2675.
[85] F. Mokhtari, M. Heidarpour, N. Zandieh, Safety of nanoparticles and evaluation of nanotoxicity, J. Bio Safety, 8 (2015) 1–10.
[86] M. Shokrzadeh, A. Tasdighi, M. Modanlo, F. Shaki, Evaluating and comparing genotoxicity mechanism of copper nanoparticles and copper sulfate, J. Mazandaran Univ. Med. Sci., 28 (2018) 1–9.
[87] M. Kermani, M. Farzadkia, A. Esrafili, Y. Shahamat, S. Jokandan, Investigation of toxicity changes of catechol in oxidation process with ozone by bioassay, Iran. J. Health Environ., 10 (2017) 237–248.
[88] S. Mashjoor, M. Alishahi, Z. Tulaby Dezfuly, Comparative toxicity assessment of chemical nanosilver and biosynthetic silver nanoparticles produced by marine macroalgae from the Persian Gulf in biomarker: *Artemia nauplii*, J. Vet. Res., 74 (2019) 73–82.
[89] K. Naddafi, M.R. Zare, M. Younesian, N. Rastkari, M. Alimohammadi, N. Mousavi, Bioassay for toxicity assessment of zinc oxide and titanium oxide to *Escherichia coli* ATCC 35218 and *Staphylococcus aureus* ATCC 25923 bacteria, Iran. J. Health Environ., 4 (2011) 171–80.
[90] H. Jin, X. Yang, D. Yin, H. Yu, A case study on identifying the toxicant in effluent discharged from a chemical plant, Mar. Pollut. Bull., 39 (1999) 122–125.
[91] M. Kermani, A. Esrafili, M. Farzadkia, S. Salahshour-Arian, Identification of oxidation intermediates and investigation of toxicity changes in heterogenic catalytic ozonation process in the presence of MgO nanoparticles for metronidazole removal from aqueous solution, J. Health Syst. Res.; Isfahan Univ. Med. Sci., 12 (2016) 140–145.
[92] G.O. El-Sayed, H.A. Dessouki, H.S. Jahin, S.S. Ibrahiem, Photocatalytic degradation of metronidazole in aqueous solutions by copper oxide nanoparticles, J. Basic Environ. Sci., 1 (2014) 102–110.

[93] O.S. Bello, O.M. Adelaide, M.A. Hammed, O.A.M. Popoola, Kinetic and equilibrium studies of methylene blue removal from aqueous solution by adsorption on treated sawdust, Macedonian Chem. Chem. Eng., 29 (2010) 77–85.
[94] N. Farnad, K. Farhadi, N.H. Voelcker, Polydopamine nanoparticles as a new and highly selective biosorbent for the removal of copper(II) ions from aqueous solutions, Water Air Soil Pollut., 223 (2012) 3535–3544.
[95] C. Wang, H. Wang, Carboxyl functionalized *Cinnamomum camphora* for removal of heavy metals from synthetic wastewater-contribution to sustainability in agroforestry, J. Cleaner Prod., 184 (2018) 921–928.
[96] C. Wang, H. Wang, Y. Cao, Pb(II) sorption by biochar derived from *Cinnamomum camphora* and its improvement with ultrasound-assisted alkali activation, Colloids Surf., A, 556 (2018) 177–184.
[97] K.J. Shiny, K.N. Remani, E. Nirmala, T.K. Jalaja, V.K. Sasidharan, Biotreatment of wastewater using aquatic invertebrates, *Daphnia magna* and *Paramecium caudatum*, Bioresour. Technol., 96 (2005) 55–58.
[98] Test No. 202: *Daphnia* sp. Acute Immobilisation Test, OECD Guidelines for the Testing of Chemicals, Section 2. 2004, OECD.
[99] S. Mashjoor, M. Aishahi, Z. Tulabi Dezfuli, Comparative toxicity assessment of chemical nanosilver and biosynthetic silver nanoparticles produced by marine macroalgae from the Persian Gulf in biomarker: *Artemia nauplii*, J. Vet. Res, 74 (2019) 73–82.
[100] R.L. Oliveira, J.G. Vieira, H.S. Barud, R. Assunção, G. R Filho, S.J. Ribeiro, Y. Messadeqq, Synthesis and characterization of methylcellulose produced from bacterial cellulose under heterogeneous condition, J. Braz. Chem. Soc., 26 (2015) 1861–1870.
[101] E. Wiercigroch, E. Szafraniec, K. Czamara, M.Z. Pacia, K. Majzner, K. Kochan, A. Kaczor, M. Baranska, K. Malek, Raman and infrared spectroscopy of carbohydrates: a review, Spectrochim. Acta, Part A, 185 (2017) 317–335.
[102] Y. Sekiguchi, C. Sawatari, T. Kondo, A gelation mechanism depending on hydrogen bond formation in regioselectively substituted O-methylcelluloses, Carbohydr. Polym., 53 (2003) 145–153.
[103] G. Rodrigues Filho, R.M.N. de Assunção, J.G. Vieira, C. da S. Meireles, D.A. Cerqueira, H. da Silva Barud, S.J.L. Ribeiro, Y. Messaddeq, Characterization of methylcellulose produced from sugar cane bagasse cellulose: crystallinity and thermal properties, Polym. Degrad. Stab., 92 (2007) 205–210.
[104] G. de Carvalho Oliveira, G.R. Filho, J.G. Vieira, R.M.N. De Assunção, C. da Silva Meireles, D.A. Cerqueira, R.J. de Oliveira, W.G. Silva, L.A. de Castro Motta, Synthesis and application of methylcellulose extracted from waste newspaper in CPV-ARI Portland cement mortars, J. Appl. Polym. Sci., 118 (2010) 1380–1385.
[105] K. Ariga, A. Vinu, Y. Yamauchi, Q. Ji, J. Hill, Nanoarchitectonics for mesoporous materials, Bull. Chem. Soc. Jpn., 85 (2012) 1–32.
[106] E. Asgari, A. Sheikhmohammadi, J. Yeganeh, Application of the Fe_3O_4-chitosan nanoadsorbent for the adsorption of metronidazole from wastewater: optimization, kinetic, thermodynamic and equilibrium studies, Int. J. Biol. Macromol., 164 (2020) 694–706.
[107] Y. Guo, W. Huang, B. Chen, Y. Zhao, D. Liu, Y. Sun, B. Gong, Removal of tetracycline from aqueous solution by MCM-41-zeolite A loaded nano zero valent iron: synthesis, characteristic, adsorption performance and mechanism, J. Hazard. Mater., 339 (2017) 22–32.
[108] N. Nasseh, L. Taghavi, B. Barikbin, M.A. Nasseri, A. Allahresani, $FeNi_3/SiO_2$ magnetic nanocomposite as an efficient and recyclable heterogeneous Fenton-like catalyst for the oxidation of metronidazole in neutral environments: adsorption and degradation studies, Composites, Part B, 166 (2019) 328–340.
[109] L. Sun, D. Chen, S. Wan, Z. Yu, Adsorption studies of dimetridazole and metronidazole onto biochar derived from sugarcane bagasse: kinetic, equilibrium, and mechanisms, J. Polym. Environ., 26 (2018) 765–777.
[110] E. Çalışkan, S. Göktürk, Adsorption characteristics of sulfamethoxazole and metronidazole on activated carbon, Sep. Sci. Technol., 45 (2010) 244–255.
[111] E.C. Lima, A. Hosseini-Bandegharaei, J.C. Moreno-Piraján, I. Anastopoulos, A critical review of the estimation of the thermodynamic parameters on adsorption equilibria. Wrong use of equilibrium constant in the Van't Hoof equation for calculation of thermodynamic parameters of adsorption, J. Mol. Liq., 273 (2019) 425–434.
[112] N. Nasseh, B. Barikbin, L. Taghavi, M.A. Nasseri, Adsorption of metronidazole antibiotic using a new magnetic nanocomposite from simulated wastewater (isotherm, kinetic and thermodynamic studies), Composites, Part B, 159 (2019) 146–156.
[113] L. Sun, D. Chen, S. Wan, Z. Yu, Adsorption studies of dimetridazole and metronidazole onto biochar derived from sugarcane bagasse: kinetic, equilibrium, and mechanisms, J. Polym. Environ., 26 (2017) 765–777.
[114] A. Nasiri, M.R. Heidari, N. Javid, G. Yazdanpanah, New efficient and recyclable magnetic nanohybrid adsorbent for the metronidazole removal from simulated wastewater, J. Mater. Sci. - Mater. Electron., 33 (2022) 25103–25126.
[115] J.L. Asensio, A. Ardá, F.J. Cañada, J. Jimenez-Barbero, Carbohydrate–aromatic interactions, Acc. Chem. Res., 46 (2013) 946–954.
[116] M. Kumari, R.B. Sunoj, P.V. Balaji, Exploration of CH π mediated stacking interactions in saccharide: aromatic residue complexes through conformational sampling, Carbohydr. Res., 361 (2012) 133–140.
[117] M. Nishio, The CH/π hydrogen bond in chemistry. Conformation, supramolecules, optical resolution and interactions involving carbohydrates, Phys. Chem. Chem. Phys., 13 (2011) 13873–13900.
[118] J. Rivera-Utrilla, G. Prados-Joya, M. Sánchez-Polo, M. Ferro-García, I. Bautista-Toledo, Removal of nitroimidazole antibiotics from aqueous solution by adsorption/bioadsorption on activated carbon, J. Hazard. Mater., 170 (2009) 298–305.
[119] D.R. Sanvordeker, Y.W. Chien, T.K. Lin, H.J. Lambert, Binding of metronidazole and its derivatives to plasma proteins: an assessment of drug binding phenomenon, J. Pharm. Sci., 64 (1975) 1797–1803.
[120] X. Zhu, J. Wang, X. Zhang, Y. Chang, Y. Chen, Trophic transfer of TiO_2 nanoparticles from *Daphnia* to zebrafish in a simplified freshwater food chain, Chemosphere, 79 (2010) 928–933.
[121] M. Hamidi, B. Jovanova, T. Panovska, Toxicological evaluation of the plant products using brine shrimp (*Artemia salina* L.) model, J. Maced Pharm. Bull., 60 (2014) 9–18.
[122] H. Azarpira, D. Balarak, Rice husk as a biosorbent for antibiotic metronidazole removal: isotherm studies and model validation, Int. J. ChemTech Res., 9 (2016) 566–573.
[123] A. Fatemeh, M. Gholami, A. Jonidi Jafari, M. Kermani, H. Asgharnia, R. Rezaei Kalantari, Study of tetracycline and metronidazole adsorption on biochar prepared from rice bran kinetics, isotherms and mechanisms, Desal. Water Treat., 159 (2019) 390–401.